

**MAGNETO-OPTICAL PROPERTIES OF ONE-DIMENSIONAL PHOTONIC
CRYSTALS**

by

Bijayandra Shakya

Submitted in partial fulfillment of the requirements

for the degree of

Master of Science in Engineering

in the

Electrical Engineering

Program

YOUNGSTOWN STATE UNIVERSITY

December 2011

**MAGNETO-OPTICAL PROPERTIES OF ONE-DIMENSIONAL PHOTONIC
CRYSTALS**

Bijayandra Shakya

I hereby release this thesis to the public. I understand that this thesis will be made available from the OhioLINK ETD Center and the Maag Library circulation desk for public access. I also authorize the University or other individuals to make copies of this thesis as needed for scholarly research.

Signature:

Bijayandra Shakya, Student Date

Approvals:

Dr. James H. Andrews, Thesis Advisor Date

Dr. Faramarz Mossayebi, Committee Member Date

Dr. Philip Munro, Committee Member Date

Peter J. Kasvinsky, Dean of School of Graduate Studies & Research Date

ABSTRACT

The magneto-optical properties of one-dimensional photonic crystals which are comprised of co-extruded alternating polymer layers of polymethyl-methacrylate (PMMA) and polystyrene (PS) are studied in this thesis. These polymers were used to experimentally test the hypothesis that Faraday rotation in a multilayer system is the sum of the rotations produced by each layer separately, themselves weighted according to the time spent in each constituent material multiplied by that material's Verdet coefficient. In the experiment, the transmissions and Faraday rotations for the monoliths of PS and PMMA films as well as a 128-layer (PS/PMMA)⁶⁴ film were measured. A 64-layer (PS/PMMA)¹⁶(PMMA/PS)¹⁶ film was also measured by simply folding a single 32-layer PS/PMMA film to create a half-wavelength defect in the center of the quarter wavelength stack. The measured Faraday rotation spectrums show enhanced Faraday rotations that are found to be consistent with the predicted Faraday rotations.

ACKNOWLEDGEMENTS

I would like to thank Dr. Philip Munro, Dr. Faramarz Mossayebi and Dr. Jalal Jalali in the Department of Electrical and Computer Engineering and Dr. James H. Andrews, Dr. Michael Crescimanno and Dr. Guilin Mao in the Department of Physics at Youngstown State University, for helping me in my thesis project. In addition, I would like to thank the National Science Foundation under Grant No. DMR 0423914 and the State of Ohio, Department of Development, State of Ohio, the Chancellor of the Board of Regents and the Third Frontier Commission, which provided funding in support of the Research Cluster on Surfaces in Advanced Materials. Finally, I would like to thank my friends and family, who helped and supported me throughout my graduate studies.

TABLE OF CONTENTS

	PAGE
ABSTRACT	iii
ACKNOWLEDGEMENTS	iv
TABLE OF CONTENTS	v
LIST OF FIGURES	vii
LIST OF SYMBOLS	ix
CHAPTER 1: INTRODUCTION	1
1.1 MAGNETO-OPTICAL PHENOMENON	1
1.2 CIRCULAR BIREFRINGENCE	4
1.3 OBJECTIVE	5
1.4 APPLICATION TO ENGINEERING	6
CHAPTER 2: ELECTRIC FIELD ENERGY DISTRIBUTION IN 1D-PC	8
2.1 ONE DIMENSIONAL PHOTONIC CRYSTALS (1D-PC)	8
2.2 INTERPRETATION OF ELECTRIC FIELD ENERGY DISTRIBUTION	9
CHAPTER 3: EXPERIMENTAL MEASUREMENT AND RESULTS	15
3.1 FARADAY ROTATION MEASUREMENT	16
3.2 RESULTS	20

CHAPTER 4: TRANSFER MATRIX APPROACHES	25
4.1 2×2 TRANSFER MATRIX APPROACHES	25
4.2 4×4 TRANSFER MATRIX APPROACHES	35
CHAPTER 5: LIMITATIONS OF TRANSFER MATRIX APPROACHES	43
CHAPTER 6: CONCLUSION	51
APPENDICES	53
APPENDIX A: REALIZATION OF 2×2 TRANSFER MATRIX APPROACHES	54
APPENDIX B: REALIZATION OF 4×4 TRANSFER MATRIX APPROACHES	64
REFERENCES	70

LIST OF FIGURES

FIGURES		PAGE
1.1	Polarization rotation due to the Faraday effect	2
2.1	General multilayer structure having m layers	9
3.1	Schematic setup of Faraday rotation experiment	15
3.2	LED used in the experiment	19
3.3	Magnet Coils used in the experiment	19
3.4	Sample (128-layer PS/PMMA) used in the experiment	20
3.5	Verdet constant spectral measurements for monoliths of PS and PMMA	21
3.6	Spectral transmission and effective Faraday rotation of 128-layer PMMA/PS	22
3.7	Spectral transmission and Faraday rotation of 64-layer folded multilayer film	24
4.1	Predicted transmission spectra of 128-layer film	30
4.2	Predicted Verdet of 128-layer film	30
4.3	Predicted transmission spectra of folded 64-layer film	31

4.4	Predicted Verdet of folded 64-layer film	31
4.5	Predicted Faraday rotation in terms of ellipticity	34
4.6	Predicted ellipticity angle in terms of scaling	35
5.1	Transmission spectrum of 16 layer PS/PMMA	43
5.2	Faraday rotation when 2nd layer is considered as special layer	44
5.3	Faraday rotation when 4th layer is considered as special layer	45
5.4	Faraday rotation when 6th layer is considered as special layer	45
5.5	Faraday rotation when 8th layer is considered as special layer	46
5.6	Faraday rotation when 10th layer is considered as special layer	46
5.7	Faraday rotation when 12th layer is considered as special layer	47
5.8	Faraday rotation when 14th layer is considered as special layer	47
5.9	Faraday rotation when 16th layer is considered as special layer	48
5.10	Faraday rotation of 8 layer PS/PMMA	49
5.11	Faraday rotation of 16 layer PS/PMMA	49
5.12	Faraday rotation of 32 layer PS/PMMA	50

LIST OF SYMBOLS

θ_F	Angle of Faraday polarization rotation (radians)
B	Magnetic field (tesla)
l	Length of the path where the light and magnetic field interact (meters)
V	Verdet constant, a property of the bulk material (radians per tesla-meter)
$\theta_F(\lambda)$	Angle of rotation as a function of wavelength λ (radians)
$V(\lambda)$	Verdet as a function of wavelength (radians per tesla-meter)
n	Refractive index of light (unitless quantity)
E	Electric field (newtons per coulomb)
c	Speed of light (meters per second)
ϵ_0	Permittivity of free space (farads per meter)
\tilde{n}_j	Complex index of refraction (unitless quantity)
r_{jk}	Complex reflection coefficient (unitless quantity)
t_{jk}	Complex transmission coefficient (unitless quantity)
$\langle \mathbf{u} \rangle$	Time average of the energy distributed in layer
I	Intensity of light (watts per meter square)

$\delta\theta_F$	Small rotation angle (degrees)
δI	Change in intensity (watts per meter square)
$I_{B\ forward}$	Light intensity when the magnetic field is parallel to the light propagating direction (watts per meter square)
$I_{B\ backward}$	Light intensity when the magnetic field is perpendicular to the light propagating direction (watts per meter square)
v_g	Group velocity (meters per second)
ω	Angular frequency of light wave (radians per second)
k	Wavenumber of light wave (per meter)
ϕ	Phase of electric field (radians)
t_D	Total time spent in multilayer system (seconds)
t_A	Time spent in layer A of the system (seconds)
t_B	Time spent in layer B of the system (seconds)
$u_{A,B}$	Electric field energy density of the multilayer system (unitless quantity)
u_A	Electric field energy density of layer A of the system (unitless quantity)
u_B	Electric field energy density of layer B of the system (unitless quantity)
χ	Ellipticity of light (radians)
ϵ	Ellipticity angle (degrees)

CHAPTER 1: INTRODUCTION

One of the most interesting research fields today is the study of magneto-optical properties of one-dimensional photonic crystals (1D-PC). This thesis studies the magneto-optical properties of multilayer polymer stacks as one-dimensional photonic crystals. Magneto-optical phenomenon is also known as Faraday rotation or Faraday effect.

1.1 MAGNETO-OPTICAL PHENOMENON

The potential applications of polymeric magneto-optic (MO) materials include attractive possibilities of more compact and integrable waveguide optical isolators and high-performance magnetic field sensors that can be readily inserted onto photonic integrated circuit platforms for both commercial and military applications [1].

The Faraday rotation is an effect caused by the interaction between electromagnetic wave (EM) and a magnetic field in a medium. The Faraday effect was discovered by Michael Faraday in 1845 and this effect was the first experimental evidence that related light and electromagnetism. Faraday rotation is the rotation of the plane of polarization of linearly polarized light due to magnetic field induced circular birefringence of a material [2]. This phenomenon is depicted in Figure 1.1. Circular birefringence is a property of the material that causes left and right circularly polarized waves to propagate at slightly different speeds. This circular birefringence property is discussed in depth in section 1.3. In a non-absorbing or weakly absorbing medium, a linearly polarized monochromatic light beam passing through a homogeneous material

along the direction of the applied magnetic field experiences circular birefringence induced by the applied magnetic field, resulting in rotation of the plane of polarization. The relation between the angle of rotation of the polarization and the magnetic field in a material is given by

$$\theta_F(\lambda) = \int_0^l V(\lambda, z) \cdot B(z) \cdot dz = V(\lambda)Bl \quad (1.1)$$

where, $\theta_F(\lambda)$ = angle of rotation as a function of wavelength (in radians)

B = magnetic field in the direction of propagation (in tesla)

l = length of the path where the light and magnetic field interact (in meters)

$V(\lambda)$ = Verdet constant as a function of wavelength (in radians/ tesla-meter)

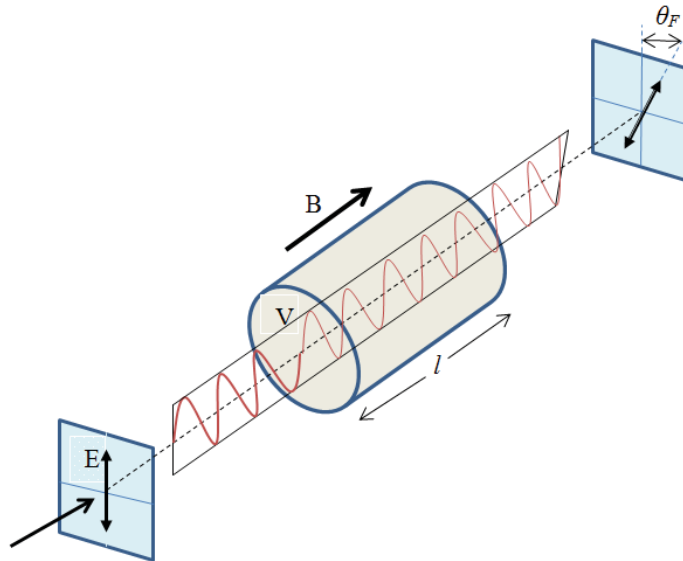


Figure 1.1: Polarization rotation due to the Faraday effect [3]

The Verdet constant is a material property that quantitatively measures the Faraday rotation of the material per unit length and unit applied magnetic field. The

Verdet constant is strongly wavelength dependent and it also depends on the magnetic field used. The Verdet constant is usually measured by determining the amount of polarization rotation that linearly polarized light experiences when incident on a sample under an ac or dc magnetic field. Faraday active materials are used in high-end applications such as optical isolators that protect lasers and optical communication devices from unwanted back reflection, highly sensitive magnetic field sensors, and satellite altitude monitors, among others [2]. Faraday rotation measurements have also been used to estimate magnetic susceptibilities and carrier densities in semiconductors where the effective mass of the carrier is known [2]. Generally, Faraday rotation is at its strongest in inorganic substances containing paramagnetic ions or in super-paramagnetic and magnetic materials. Unfortunately, these materials are often very expensive and difficult to process and/or are not suitable for applications at ambient temperatures. Organic or polymeric materials had not been investigated for efficient Faraday rotation until recently. Nevertheless, a significant advantage of organic materials would be their ease of processing, limited weight, and the fact that they can be custom designed and synthesized to meet specific device requirements [2].

In a practical description of Faraday rotation in a non-birefringent bulk material, the angle of rotation θ_F is a function of wavelength λ and depends upon the transport length through the medium as seen in Eq. (1.1).

It is obvious that when there are multilayer reflections Eq. (1.1) does not apply because the transport length depends upon the multiple reflections within the material. The Faraday rotation is non-reciprocal (i.e., the direction of rotation of the polarization, either clockwise or counter-clockwise, is the same whether the light is travelling

backward or forward with respect to the applied magnetic field). In the vicinity of the reflection band (range of wavelengths where the light is not allowed to permit) of a photonic crystal, a different approach is required to account for the increased interaction due to forward and backward reflections within the entire multilayer stack. This can be accomplished through a standard treatment for a one-dimensional photonic crystal using 4×4 transfer matrix formulation that combines the polarization rotation effects of each layer in the multilayer stack.

1.2 CIRCULAR BIREFRINGENCE

The rotation of the polarized light wave passing through the electronic structure is the result of field induced circular birefringence – the existence of different refractive indices for left circularly and right circularly polarized light components. Each component traverses the sample with different refractive indices and therefore with a different speed. The end consequence consists of left circularly and right circularly polarized light components that are out of phase and their superposition is linearly polarized light rotated with respect to its original direction.

The Verdet constant is given in the simple model as [4]

$$V \propto \lambda \frac{dn}{d\lambda} \quad (1.3)$$

where, λ = wavelength

$$\frac{dn}{d\lambda} = \text{dispersion of index of refraction}$$

Eq. (1.3) shows that Verdet constant is proportional to both the wavelength and the dispersion of the index of refraction.

1.3 OBJECTIVE

Although this thesis is a study of one-dimensional photonic crystals as experimental Faraday rotators (in this instance, alternating layers of polymethylmethacrylate (PMMA) and polystyrene (PS)), it is not intended for device fabrication because the inherent Faraday rotation of these materials, as indicated by their Verdet Constants, is very small. But there has been major technological progress in the use of multilayer materials as optical rotators, including the theoretical studies in the past few decades. These one-dimensional photonic crystals have been modeled and measured using various multilayer configurations consisting of one or two distinct dielectric materials (A, B) and one or two magnetic materials (M), typically iron garnet and other magnetically enhanced materials layered with inorganic dielectric glasses. Layered systems studied include magnetic materials sandwiched within a distributed Bragg structure $(AB)^a M (BA)^b$ [5, 6, 7, 8, 9] or magnetic materials alternated with dielectrics as in $(MA)^a$ or $(MA)^a M^b (MA)^a$ [10, 11, 12, 13, 14, 15], $(MA)^a (AM)^b (MA)^a$ [16, 17], $(M_1 M_2)^a$ or even purely magnetic bilayers as in $(M_1 M_2)^a M_1^b (M_2 M_1)^a$ [18, 19]. Here, for simplicity, superscripts a and b represent any number of layers and, in some cases, half layers, where the layers in parenthesis may be permuted in either order.

This thesis also describes a quantitative time-based theory for Faraday rotation that relies on the 2×2 transfer matrix formulation (i.e., the transport of a single polarization in the absence of the Faraday effect only). The solution of the transport for

this single polarization is then used to determine the transport time through each layer of the multilayer stack. This concludes that the Faraday rotation from one-dimensional photonic crystals can then be written as simply the sum of the products of the time spent in each layer by the Verdet constant for that material (written in time units). This conclusion is further supported by comparing its results with the results from the 4×4 transfer matrix theory.

The MATLAB program has been used to simulate and compare the theoretical aspects of 4×4 transfer matrix and 2×2 transfer matrix. The data from the MATLAB program are imported in Microsoft Excel program for further calculations and verifications.

The main objective of this thesis is to measure the Faraday rotation of one dimensional photonic crystals using transfer matrix approaches as these approaches give simple and quantitative physical picture for the connection between transport and Faraday rotation that may be useful for the scientists to optimize the structure-property relationships of one-dimensional photonic crystals.

1.4 APPLICATION TO ENGINEERING

Faraday rotation has many applications in Engineering. An optical current transformer (CT) can be developed based on the principle of the Faraday effect and the information measured by the optical CT can be transmitted to the ground side substations through optical fibers contained in an insulator [20]. With suitable analysis, one can obtain information on spatial profiles of magnetic field fluctuations via Faraday rotation. Coherent interaction between these fluctuations can be measured to generate an

electromagnetic torque [21]. The sensitivity of an optical current sensor can be improved with the enhancement of Faraday rotation. This serves as a tool to design and analyze practical optical current sensors [22]. Faraday rotation is obtained in highly birefringent single-mode fibers by using alternating or periodically spaced regions of magnetic field. This approach has potential applications in isolators, circulators, combination tuning and unidirectional elements, and for studying fiber birefringence [23].

CHAPTER 2: ELECTRIC FIELD ENERGY DISTRIBUTION IN 1D-PC

Photonic crystals are made up of periodic dielectrics (i.e., an electrical insulator that can be polarized by an applied electric field) that affect the propagation of electromagnetic waves (EM). Basically, photonic crystals comprise frequently repeating internal regions of high and low dielectric constant. The propagation of photons, acting as waves, depends upon their wavelength. The wavelengths of light that are permitted to travel are known as modes, and the ranges of wavelengths that are not permitted to travel are called photonic band gaps.

2.1 ONE DIMENSIONAL PHOTONIC CRYSTALS (1D-PC)

The simplest possible photonic crystal consists of alternating layers of material with different dielectric constants: a multilayer film. One dimensional photonic crystal, also called a Bragg crystal, is the system that consists of alternating layers of materials with different dielectric constants where the dielectric function varies along one direction only [24].

There are different approaches to obtain the reflection and transmission coefficients of the electromagnetic field in the multilayer system. One of the approaches for multilayer system is to use matrix methods. “The multilayer system with isotropic and homogenous media and parallel-plane interfaces can be described by 2×2 matrices due to the fact that the equations governing the propagation of the electric field are linear and that the tangential component of the electric field is continuous.” [25]

2.2 INTERPRETATION OF ELECTRIC FIELD ENERGY DISTRIBUTION

A plane wave incidents from left at a multilayer system having m layers between a semi-infinite transparent ambient and a semi-infinite substrate as schematically described in Figure 2.1

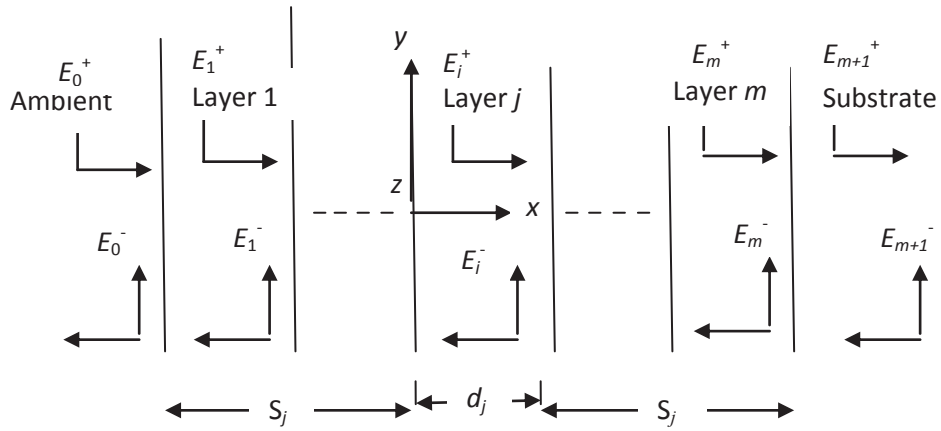


Figure 2.1: General multilayer structure having m layers
(reprinted from Ref. [25])

Each layer j ($j = 1, 2, \dots, m$) has thickness d_j and its optical properties are described by its complex index of refraction $\tilde{n}_j = \eta_j + ik_j$ which is a function of wavelength (energy) of the incident wave [25]. (Here, $i = \sqrt{-1}$ is used to represent a complex number)

The electric field at any point in the system can be resolved into two components equivalent to the resultant total electric field; one component propagating in the positive x -direction and the other in the negative x -direction. These components at a position x in layer j are denoted by $E_j^+(x)$ and $E_j^-(x)$ along positive and negative x -directions

respectively. An interface matrix (i.e, matrix of refraction) for each interface in the structure can be described as [25]

$$\mathbf{I}_{jk} = \frac{1}{t_{jk}} \begin{bmatrix} 1 & r_{jk} \\ r_{jk} & 1 \end{bmatrix} \quad (2.1)$$

where, r_{jk} and t_{jk} are the complex reflection coefficient and transmission coefficient at interface jk respectively.

We assume that the direction of propagation of light is normally incident on the multilayer structure. In this case, the complex reflection and transmission coefficients are defined by

$$r_{jk} = \frac{n_j - n_k}{n_j + n_k} \quad (2.2)$$

$$t_{jk} = \frac{2n_j}{n_j + n_k} \quad (2.3)$$

The layer matrix (or phase matrix) describing the propagation through layer j is described by

$$\mathbf{L}_j = \begin{bmatrix} e^{-i\xi_j d_j} & 0 \\ 0 & e^{i\xi_j d_j} \end{bmatrix} \quad (2.4)$$

where

$$\xi_j = \frac{2\pi}{\lambda} n_j \quad (2.5)$$

and

$\xi_j d_j$ = layer phase thickness corresponding to the phase change the wave experiences as it traverses layer j [25].

By utilizing the interface matrix and layer matrix of Eq. (2.1) and Eq. (2.4), the relation between the total system transfer matrix \mathbf{S} (or scattering matrix) and electric field at ambient side and substrate side is given by [25]

$$\begin{pmatrix} E_0^+ \\ E_0^- \end{pmatrix} = \mathbf{S} \begin{pmatrix} E_{m+1}^+ \\ E_{m+1}^- \end{pmatrix} \quad (2.6)$$

Also,

$$\mathbf{S} = \begin{bmatrix} S_{11} & S_{12} \\ S_{21} & S_{22} \end{bmatrix} = \left(\prod_{v=1}^m I_{(v-1)} L_v \right) I_{m(m+1)} \quad (2.7)$$

When the wave is incident from the ambient side in the positive x -direction there is no wave propagating in the negative x -direction inside the substrate, which means that $E_{m+1}^- = 0$. For the total layered structure the resulting complex reflection and transmission coefficients can be expressed by using the matrix elements of the total system transfer matrix of Eq. (2.7) as [25]

$$r = \frac{E_0^-}{E_0^+} = \frac{S_{21}}{S_{11}} \quad (2.8)$$

$$t = \frac{E_{m+1}^+}{E_0^+} = \frac{1}{S_{11}} \quad (2.9)$$

In order to calculate the internal electric field in layer j the layer system is divided into two subsets, separated by layer j . Thus, the total system transfer matrix can be written as [25]

$$\mathbf{S} = \mathbf{S}'_j \mathbf{L}_j \mathbf{S}''_j \quad (2.10)$$

The partial system transfer matrices for layer j are defined as [25]

$$\begin{pmatrix} E_0^+ \\ E_0^- \end{pmatrix} = \mathbf{S}'_j \begin{pmatrix} E_j^+ \\ E_j^- \end{pmatrix}, \quad (2.11)$$

$$\mathbf{S}'_j = \begin{bmatrix} S'_{j11} & S'_{j12} \\ S'_{j21} & S'_{j22} \end{bmatrix} = (\prod_{v=1}^{j-1} \mathbf{I}_{(v-1)} \mathbf{L}_v) \mathbf{I}_{(j-1)j} \quad (2.12)$$

where E_j^+ and E_j^- refer to the left boundary $(j-1)j$ of layer j and

$$\begin{pmatrix} E_j^{''+} \\ E_j^{''-} \end{pmatrix} = \mathbf{S}''_j \begin{pmatrix} E_{m+1}^+ \\ E_{m+1}^- \end{pmatrix}, \quad (2.14)$$

$$\mathbf{S}''_j = \begin{bmatrix} S''_{j11} & S''_{j12} \\ S''_{j21} & S''_{j22} \end{bmatrix} = (\prod_{v=j+1}^m \mathbf{I}_{(v-1)} \mathbf{L}_v) \cdot \mathbf{I}_{m(m+1)} \quad (2.15)$$

where, $E_j^{''+}$ and $E_j^{''-}$ refer to the right boundary $j(j+1)$ of layer j .

Also for the partial systems \mathbf{S}'_j and \mathbf{S}''_j , the complex reflection and transmission coefficients for layer j can be defined in terms of the matrix elements as [25]

$$r'_j = \frac{S'_{j21}}{S'_{j11}} \quad (2.16)$$

$$t'_j = \frac{1}{S'_{j11}} \quad (2.17)$$

$$r''_j = \frac{S''_{j21}}{S''_{j11}} \quad (2.18)$$

$$t_j'' = \frac{1}{S_{j11}''} \quad (2.19)$$

The relation between an internal transfer coefficient and incident plane wave to the internal electric field propagating in the positive x -direction in layer j at interface $(j - 1)j$ can be derived as [25]

$$t_j^+ = \frac{E_j^+}{E_0^+} = \frac{t_j'}{1 - (r_{j-}' - r_j'' e^{i2\xi_j d_j})} \quad (2.20)$$

where,

$$r_{j-}' = -\frac{S_{j12}'}{S_{j11}'} \quad (2.21)$$

Similarly, the relation between an internal transfer coefficient and incident plane wave to the internal electric field propagating in the negative x -direction in layer j at interface $(j - 1)j$ can also be derived as [25]

$$t_j^- = \frac{E_j^-}{E_0^+} \frac{t_j' r_j'' e^{i2\xi_j d_j}}{1 - (r_{j-}' r_j'' e^{i2\xi_j d_j})} = t_j^+ r_j'' e^{i2\xi_j d_j} \quad (2.22)$$

Using Eq. (2.20) and Eq. (2.22), the total electric field in an arbitrary plane in layer j at a distance x to the right of boundary $(j - 1)j$ in terms of the incident wave E_0^+ is given by [25]

$$\begin{aligned}
E_j(x) &= E_j^+(x) + E_j^-(x) \\
&= [t_j^+ e^{i\xi_j x} + t_j^- e^{-i\xi_j x}] E_0^+ \\
&= t_j^+ [e^{i\xi_j x} + r_j'' e^{-i\xi_j(2d_j - x)}] E_0^+
\end{aligned} \tag{2.23}$$

The expression in Eq. (2.23) is true for $0 \leq x \leq d_j$ and can be expressed in terms of the matrix elements of the partial system transfer matrices as [25]

$$E_j(x) = \frac{S_{j11}'' e^{-\xi_j(d_j - x)} + S_{j21}'' e^{\xi_j(d_j - x)}}{S_{j11}' S_{j11}'' e^{-\xi_j d_j} + S_{j12}' S_{j21}'' e^{\xi_j d_j}} E_0^+ \tag{2.24}$$

The time average of the energy distributed in layer j at position x at normal incidence is given by

$$\langle u \rangle \propto \eta_j^2 |E_j(x)|^2 \tag{2.25}$$

Eq. (2.25) illustrates that the energy density at position x in the layered structure is proportional to the product of the modulus squared of the electric field $|E_j(x)|^2$ and the refractive index η_j .

CHAPTER 3: EXPERIMENTAL MEASUREMENT AND RESULTS

An experimental setup was built to determine the Faraday rotation of multilayer films. The Faraday rotation spectra of a sample test glass (BK7), constituent polymer monoliths and the multilayer films are discussed.

3.1 FARADAY ROTATION MEASUREMENT

The schematic setup of Faraday rotation experiment is shown in Figure 3.1.

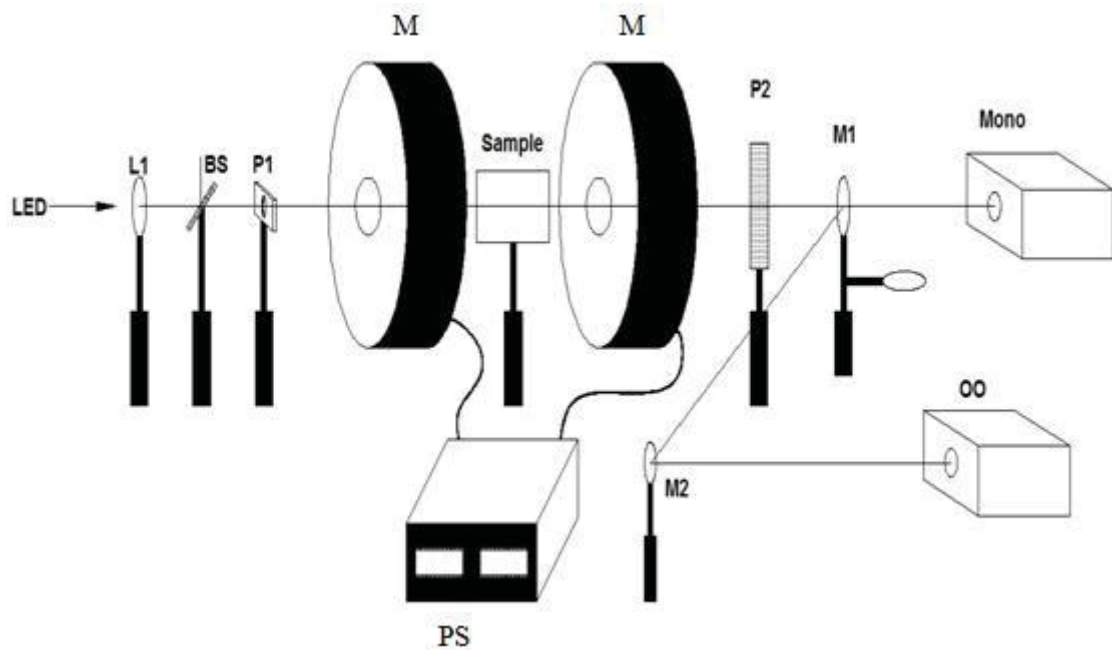


Figure 3.1: Schematic setup of Faraday rotation experiment

Where, LED = High lumen green LED

L1 = Collimation Lens

BS = Beam Splitter

P1 = Thin film polarizer

P2 = Thin film polarizer/analyzer mounted on rotary mount

M = Magnet

PS = Power Supply

M1 & M2 = Mirrors

Mono = Monochromator

OO = Ocean Optics CCD

In the experiment, Faraday rotation was measured by the light transmitted through a sample placed between a polarizer and analyzer in the presence of a magnetic field as shown in Figure 3.1.

The intensity of a light source after the analyzer P2 could be written as

$$I_1 = I_0 \cos^2(\theta) \quad (3.1)$$

where, I_0 = initial intensity

θ = angle between the initial input polarizer immediately prior to the sample and analyzer immediately following the sample.

When a magnetic field was applied, the intensity change caused by the Faraday rotation could be written for small rotation angle $\delta\theta$ as

$$\delta I_1 = -I_0 \sin(2\theta) \delta\theta \quad (3.2)$$

[Eq. (3.2) is calculated by taking the derivatives of Eq. (3.1) with respect to θ]

It was obvious from Eq. (3.2) that δI_1 was maximum when $\theta = 45^\circ$. Even though the rotation signal was maximized at 45° , the analyzer angle was found not to be optimal for measuring Faraday rotation when one was measuring very small rotations.

Dividing Eq. (3.2) by Eq. (3.1), the rotation angle could be expressed as

$$\delta\theta = -\frac{1}{2 \tan(\theta)} \frac{\delta I}{I_1} \quad (3.3)$$

From Eq. (3.3), it was obvious that the angle θ played a significant role in determining the sensitivity of a Faraday rotation measurement, i.e., how small of a rotation angle could be measured. The light stability of the system ultimately limited the sensitivity of the Faraday rotation measurement.

When $\theta = 45^\circ$ then $\delta\theta \approx -0.5 \frac{dI_1}{I_1}$ and 1% variation in the light intensity corresponded to a maximum rotation angle resolution sensitivity of $\pm 0.3^\circ$. However, when a larger angle was used (for example, $\theta = 85^\circ$), then $\delta\theta \approx -22.8 \frac{dI_1}{I_1}$ and the resolving capability was increased by a factor of 11.4. To make the sample measurements the analyzer was kept at either 85° or 88° with respect to the polarizer, depending upon the amount of light transmitted through the sample. The stability of the experimental setup allowed measured rotations as small as 0.002° with a resolution of 0.001° .

Instead of measuring the change in light intensity arising from switching on and off the magnet (greater than 1.0 Tesla), the signal between balanced forward and backward longitudinal magnetic fields was measured. Using equal forward and backward

applied magnetic fields offered two advantages: (1) the amplitude of the resulting signal was doubled, and (2) quadratic effects, including the mechanical noise caused by strong magnetic field were eliminated, much as would be the case with an ac detection system [26]. Within the limits of the system, the larger magnetic fields were achieved and better resolution was obtained through the use of dc magnetic fields. The resulting modification of Eq. (3.3) was shown in Eq. (3.4).

$$\theta_F = - \frac{1}{2 \tan(\theta)} \frac{I_{B \text{ forward}} - I_{B \text{ backward}}}{I_{B \text{ forward}} + I_{B \text{ backward}}} \quad (3.4)$$

where, $I_{B \text{ forward}}$ = light intensity when field is parallel to the light propagating direction

$I_{B \text{ backward}}$ = light intensity when field is perpendicular to the light propagating direction

Because of the small signals being measured, the stability of the intensity of the light source needed to be better than 0.1%. A 20W high lumen broadband LED (shown in Figure 3.2) was used as the light source operating at a constant current of 25A. The ice-water cooled LED showed a broad emission spectrum of wavelengths from 450 nm to 600 nm. The thin film polarizers which were used on each side of 1.0 tesla magnet coils (shown in Figure 3.3) were kept at a distance of 53 cm from the magnet. The sample (shown in Figure 3.4) was mounted on a non-magnetic holder between two coils. A monochromator with resolution of 2.5 nm was used to choose the wavelength range incident on the detectors for each measurement. The relatively low resolution was necessitated by the low light levels present at the detector, especially far from the LED's peak output and deep within the reflection band of our multilayers. Two intensity-to-

frequency converters (Type TSL237) were used as light detectors because of their stability, linearity, dynamic range and ease of use. [The TSL237 converter is a combination of a silicon photodiode and a current-to-frequency converter on a single monolithic CMOS integrated circuit. The output from the TSL237 converter is a square wave (50% duty cycle) with frequency directly proportional to light intensity.]

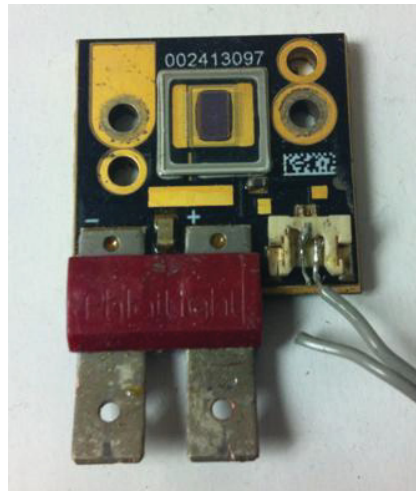


Figure 3.2: LED used in the experiment

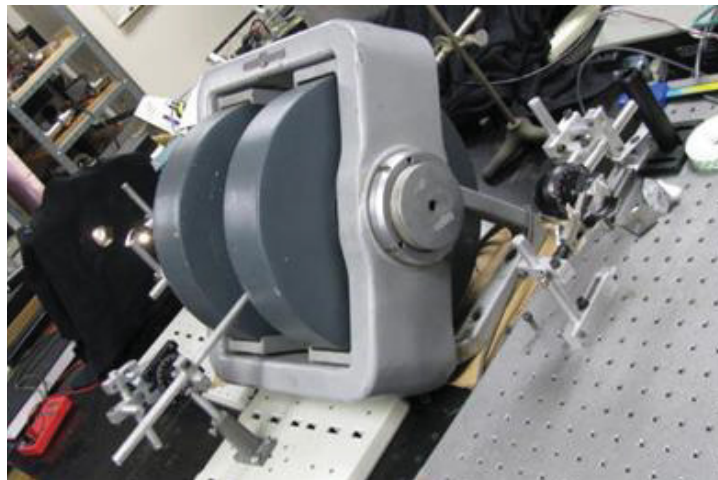


Figure 3.3: Magnet Coils used in the experiment



Figure 3.4: Sample (128-layer PS/PMMA) used in the experiment

3.2 RESULTS

In order to check the experimental setup, the Verdet coefficients of BK7 glass were measured. A 4mm thick BK7 glass slab was measured at $\theta = 45^\circ$ because this thickness produced large polarization rotation when compared to the polymer monoliths and a multilayer sample. The Verdet constant was found to be $V = 8.0 \pm 0.1$ Rad/ (T-m) at 491nm, which agreed with the spectrally adjusted value [$V = 7.7$ Rad/ (T-m) at 491nm] in the literature for this wavelength [27].

The thicknesses of the PMMA and PS monolith films that were measured were 220 μm and 208 μm respectively. These films were characterized at $\theta = 80^\circ$ and were scanned from 450 nm to 600 nm. The measured spectrum is shown in Figure 3.2.

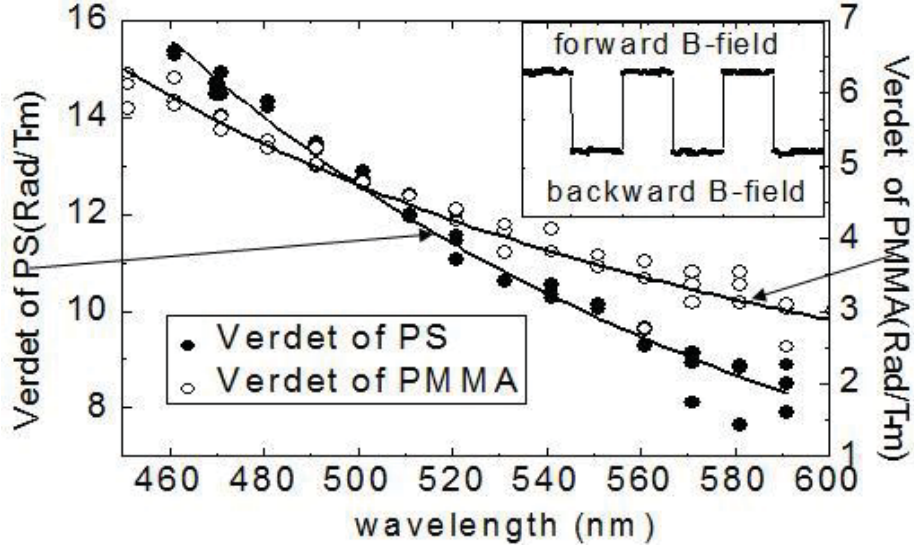


Figure 3.5: Verdet constant spectral measurements for monoliths of PS and PMMA

The inset on the top right of Figure 3.5 showed an example of the experimental data that were collected for forward and backward applied magnetic fields. At each wavelength, the light intensity was integrated for 150 seconds with the forward field and then 150 seconds with the backward field and each measurement was then repeated three times. The solid circles and open circles in Figure 3.5 are the experimentally determined values of the PS Verdet constant and the PMMA Verdet constant, respectively. Both these values were fitted with the modified Cauchy Becquerel dispersion model [28]

$$V = \frac{a}{\lambda^2} + \frac{b}{\lambda^4} \quad (3.5)$$

where, λ = wavelength in meters

a, b = fitting parameters

$a = 7.40 \times 10^5 \text{ m}^2\text{T}^{-1}$, $b = 1.10 \times 10^{11} \text{ m}^4\text{T}^{-1}$ for PMMA

$a = 2.27 \times 10^6 \text{ m}^2\text{T}^{-1}$, $b = 2.21 \times 10^{11} \text{ m}^4\text{T}^{-1}$ for PS

The Verdet value for PMMA was found to be 3.6 Rad/(T-m) at 550 nm and that for PS was found to be 14 Rad/(T-m) at 488 nm, which closely agreed with literature values [For PMMA, $V = 3.5$ Rad/(T-m) at 550 nm and for PS, $V = 15.5$ Rad/(T-m) at 488 nm] [29, 30].

Then a 128 layer PMMA/PS multilayer film of thickness 11 μm was measured. The transmission spectrum for our film was measured using Ocean Optics USB4000 spectrometer and the sample's reflection band was centered at 505 nm. The Faraday rotation spectrum was measured at $\theta = 88^\circ$ and the rotation values were calibrated at 491 nm with the analyzer setting at $\theta = 85^\circ$. The Faraday rotation angles were also corrected by subtracting the measured rotation angle without the presence of sample. The results are shown as a function of incident wavelength in Figure 3.6.

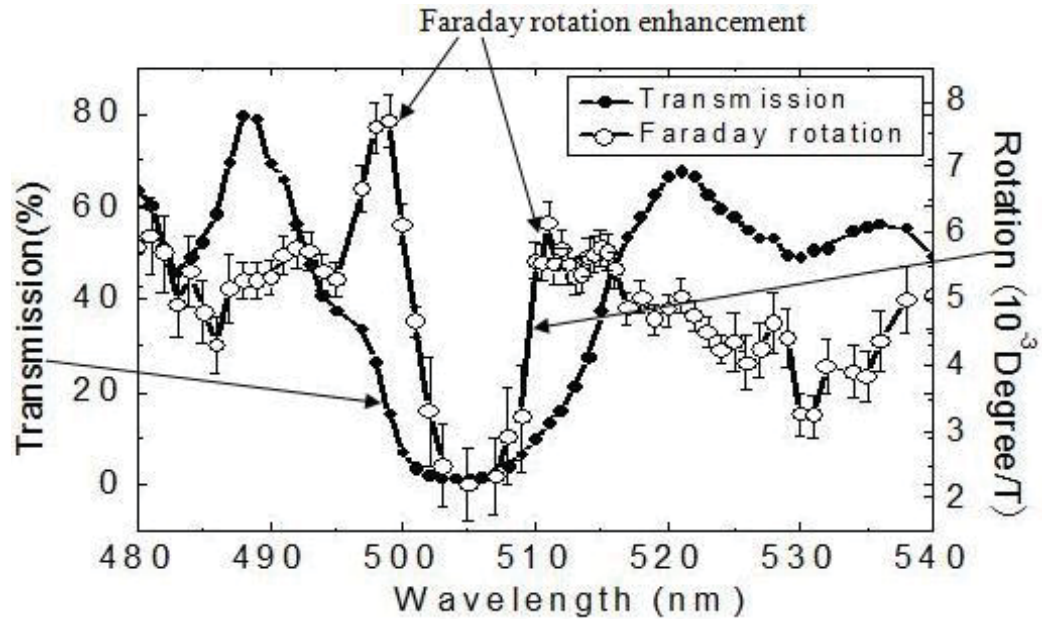


Figure 3.6: Spectral transmission and effective Faraday rotation of 128-layer PMMA/PS

The Faraday rotation spectrum obtained in Figure 3.6 showed that outside of the reflection band region (497 nm to 513nm), the experimental value for the multilayers was close to the average value for combined PMMA and PS monoliths of the same total thickness as our multilayers, which was logical because multi-reflection interference effects in the off-band range were weak. On the other hand, the effective Verdet constant dropped inside the reflection band. Near the left edge of the band, a clear peak showed an enhancement by a factor of about 1.5. On the right edge, the enhancement was also present, but at a significantly lower level. It could be noted that the maximum enhancement was appeared to be close to the value for a monolith of the PS but the modeling and additional measurements verified that this was not a general result. With a multilayer system of higher uniformity and with a detection scheme of narrower wavelength spread, the Faraday rotation for the multilayer film would exceed the value for an equally thick monolith of the higher Verdet material alone.

As a confirmation and further investigation of both reflection band-edge and band defects, a folded multilayer film comprised of two 32-layer PS/PMMA structures configured as $(\text{PS/PMMA})^{16}(\text{PMMA/PS})^{16}$ was measured. The results are shown in Figure 3.7.

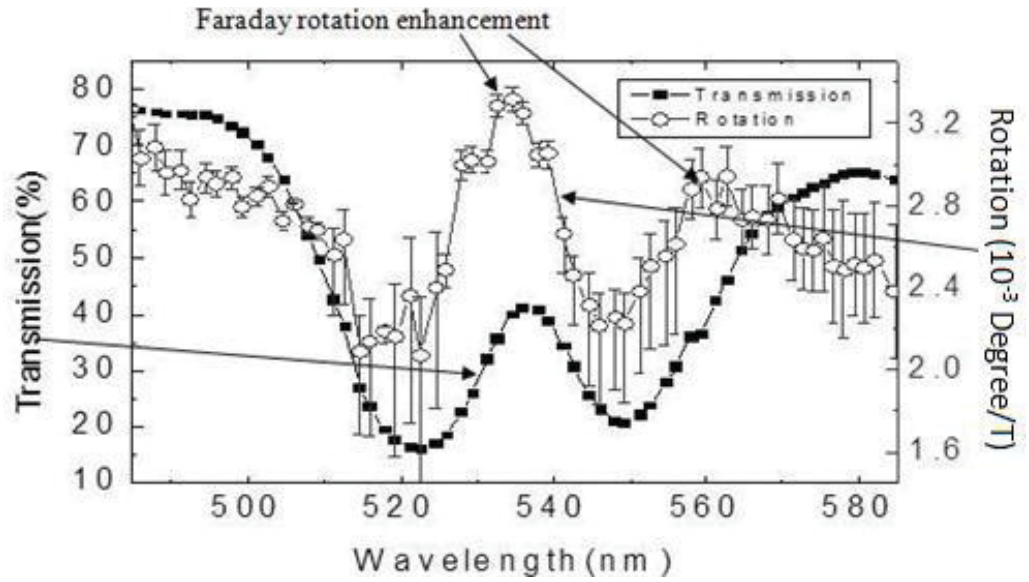


Figure 3.7: Spectral transmission and Faraday rotation of 64-layer folded multilayer film

The Faraday rotation spectrum from Figure 3.7 illustrates that the central transmission region splitting the reflection band (505 nm to 565 nm) corresponds to a region of enhanced effective Verdet 1.5 times that of a monolithic structure based on an average of the Verdet constants of the two constituent species. The edge enhancement on the long wavelength side of the reflection band can also be seen.

CHAPTER 4: TRANSFER MATRIX APPROACHES

In this chapter, a theoretical explanation of the experimental results and an alternative way to quantitatively understand the Faraday rotation in the multilayer system in terms of time spent in the various species making up the system, are described. Even though this alternative approach requires significant computation, it defines the role of the magneto-optical phenomenon of the member species. This approach may be helpful for studying that multilayer system that has larger Verdet than we studied. However, transfer matrix approaches have some limitations, which are discussed in Chapter 5.

4.1 2×2 TRANSFER MATRIX APPROACH

A 4×4 transfer matrix approach is a standard approach to quantitatively determine the optical properties of the multilayer system representing boundary matching and transport for each layer. The 4×4 transfer matrix approach is discussed in detail in section 4.2. Even though this approach is satisfactory, we propose that it does not clarify the physical characteristics of magneto-optical rotation across the reflection stop band or at band defects. An alternative approach is 2×2 transfer matrix which emphasizes the transport for each layer in time rather than in space. This 2×2 transfer matrix approach is simple because it highlights the transport of a single polarization. The 2×2 transfer matrix approach is realized in Appendix A.

The bulk Verdet coefficients V per unit length L of a multilayer system can be expressed in terms of reduced Verdet coefficients v per unit time t . In practice,

$$v = V v_g \quad (4.1)$$

where, v = reduced Verdet coefficients

V = bulk Verdet coefficients

$v_g = \frac{\partial \omega}{\partial k}$ is the group velocity (velocity of wave with which the overall shape of the wave's amplitudes propagates through space).

To determine the Faraday rotation, we need to calculate the time spent in each layer of the system and multiply that with the layer's Verdet (in time units). However, in multilayer system, the time spent in each layers is not a straightforward function of the thickness of the layer because the net effect of boundary conditions at each interface greatly influences the time. For simplicity, the rotation angle per tesla can be expressed as

$$\frac{\theta_F}{B_{\text{-field}}} = \sum_{\text{all layers}} V v_g t_D = (V v_g)_A t_A + (V v_g)_B t_B = v_A t_A + v_B t_B \quad (4.2)$$

Where, subscripts A and B indicate the two constituent species of the system and t_A and t_B are the time spent in each species.

The total time spent in the multilayer system can be computed as $t_D = t_A + t_B$, and in terms of group velocity,

The group velocity of the light wave in the multilayer system is given by

$$v_g = \frac{\partial \omega}{\partial k} \quad (4.3)$$

where, ω = angular frequency of light wave

k = wavenumber (i.e., property of light wave)

The phase of the transmitted electric field with respect to the incoming electric field as a function of the wavelength λ is given by

$$\phi = kl \quad (4.4)$$

where, l = distance travelled by the light wave

The total time spent by the light in the multilayer system is

$$t_D = \frac{l}{v_g} = l \frac{\partial k}{\partial \omega} = \frac{\partial \phi}{\partial \omega} \quad (4.5)$$

Also,

$$\frac{\omega}{k} = c \quad (4.6)$$

where, c = speed of light

Solving Eq. (4.5) and Eq. (4.6),

$$t_D = \frac{1}{c} \frac{\partial \phi}{\partial k} \quad (4.7)$$

$$t_D = \frac{1}{c} \frac{\partial \phi}{\partial \lambda} \frac{\partial \lambda}{\partial k} \quad (4.8)$$

The wavenumber is given by

$$k = \frac{2\pi}{\lambda} \quad (4.9)$$

Differentiating Eq. (4.9),

$$\frac{\partial \lambda}{\partial k} = -\frac{2\pi}{k^2} \quad (4.10)$$

Substituting $\frac{\partial \lambda}{\partial k}$ in Eq. (4.8),

$$t_D = \frac{2\pi}{ck^2} \frac{\partial \phi}{\partial \lambda} \quad (4.11)$$

$$t_D = \frac{\lambda^2}{2\pi c} \frac{d\phi}{d\lambda} \approx \frac{\lambda^2}{2\pi c} \frac{\phi}{\lambda} \quad (4.12)$$

The simple way to allocate t_D into t_A and t_B is by reference to the probability of finding the photon in one species or the other. Hence, the 2×2 transfer matrix approach is used to calculate the local energy density contours for the multilayer system by dividing each layer into sublayers (ten sublayers in our case) and summing the electric field energy density $u_{A,B} = \sum(n^2 E^2)_{A,B}$, for each species over its sublayers [31]. These energy densities correspond to the probability of finding a photon at each point in the stack and thus are used to determine the time spent in each species i.e.,

$$t_A = \frac{u_A t_D}{u_A + u_B} \quad (4.13)$$

$$t_B = \frac{u_B t_D}{u_A + u_B} \quad (4.14)$$

Then, t_A and t_B are weighted by V and v_g

$$\text{Here, } v_g = \frac{c}{n} \left(1 + \frac{\lambda}{n} \left(\frac{dn}{d\lambda} \right) \right) \quad (4.15)$$

Thus, the Faraday rotation per applied magnetic field ($B_{\text{-field}}$) for the entire multilayer system is given by

$$\frac{\theta_F}{B_{\text{-field}}} = v_A t_A + v_B t_B = \frac{(V v_g)_A \sum_{A \text{ layers}} (nE)^2 + (V v_g)_B \sum_{B \text{ layers}} (nE)^2}{\sum_{All \text{ layers}} (nE)^2} \quad (4.16)$$

To connect the results of our modeling to our experimental results, we begin with the values for the bulk Verdet spectral dispersion formula obtained by fitting bulk Verdet constants reported elsewhere in the literature for PMMA [30] and PS [29].

In our calculation, the Cauchy refractive index dispersion was used

$$n^2(\lambda) = n_{\lambda=\infty}^2 + \frac{c_1}{\lambda^2} \quad (4.17)$$

where, the two parameters $n_{\lambda=\infty}^2$ and c_1 correspond to 2.4 and 8.31×10^4 for PMMA and 2.61 and 6.14×10^4 for PS respectively, with c_1 in nm^2 [32,33].

Using this approach, we calculated the transmission and Faraday rotation $\frac{\theta_F}{B_{\text{-field}}}$ in our 128-layer and folded 64-layer PMMA/PS polymer.

The results of our modeling are shown in Figure 4.1, Figure 4.2, Figure 4.3 and Figure 4.4. Figure 4.1 and Figure 4.3 show the transmissions and Figure 4.2 and Figure 4.4 show the Faraday rotations per applied field using both the 4×4 approach (dotted lines) and the 2×2 approach (thin solid lines).

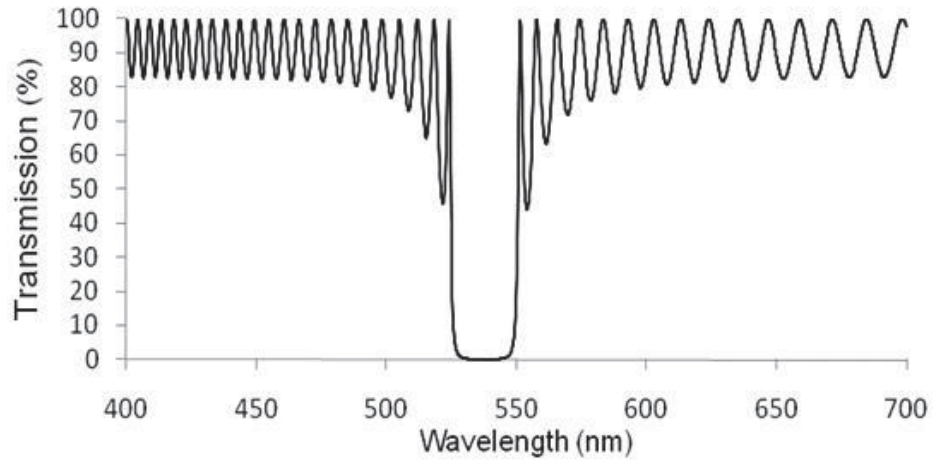


Figure 4.1: Predicted transmission spectra of 128-layer film

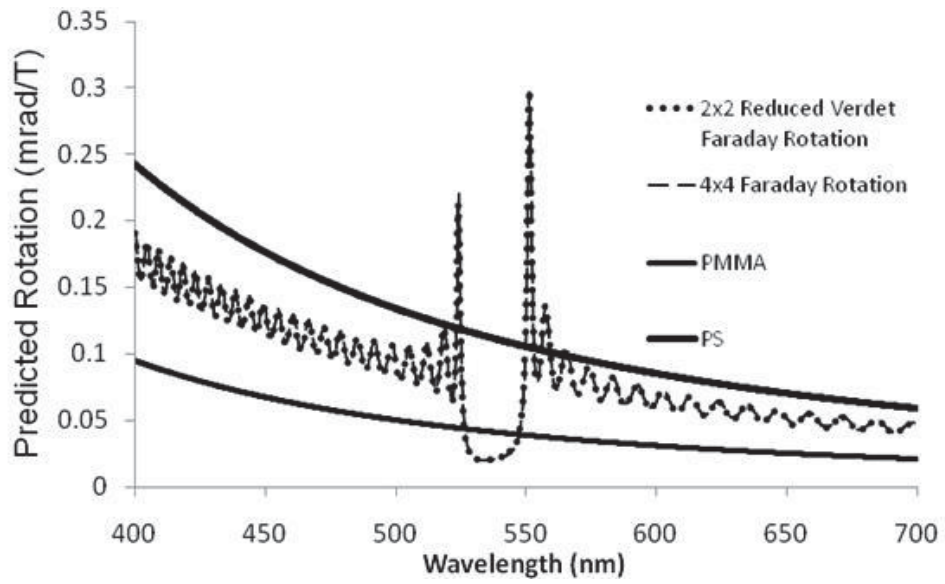


Figure 4.2: Predicted Verdet of 128-layer film

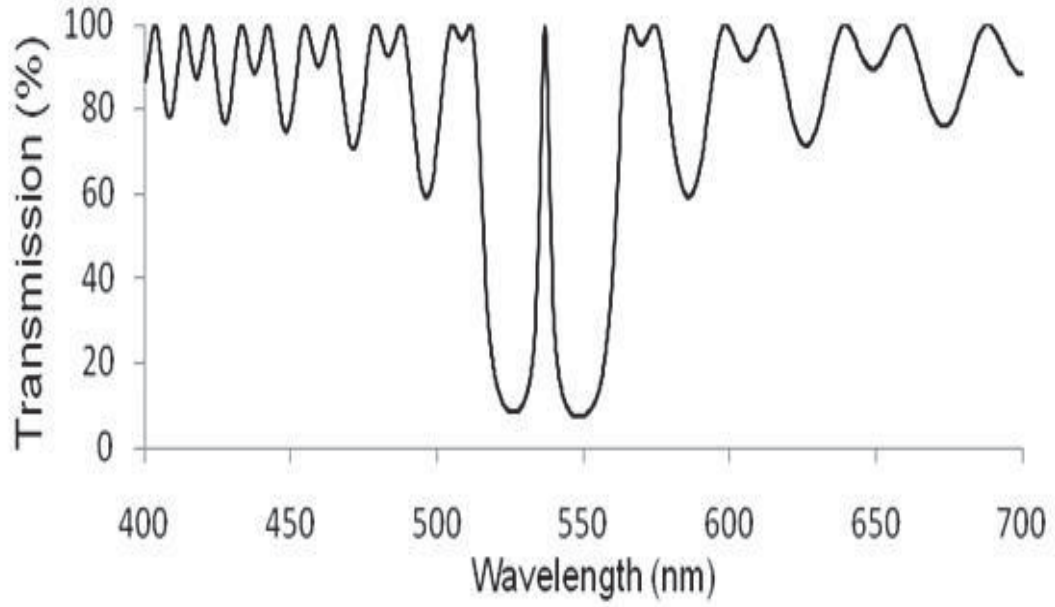


Figure 4.3: Predicted transmission spectra of folded 64-layer film

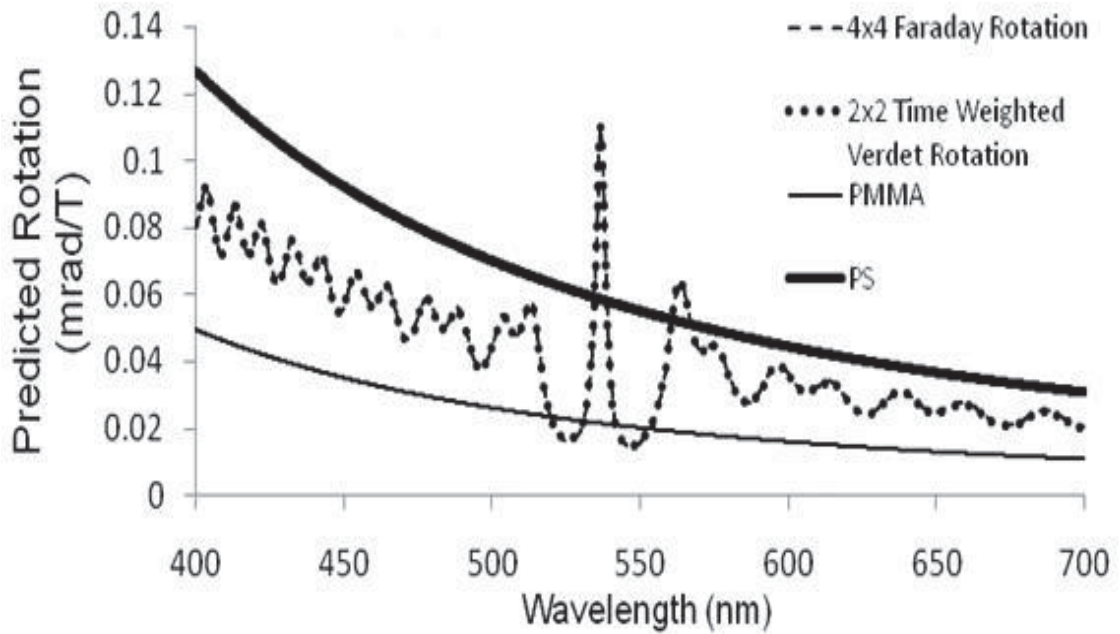


Figure 4.4: Predicted Verdet of folded 64-layer film

Figure 4.1 and Figure 4.2 are calculated for the 128 layer (PS/PMMA)⁶⁴ structure and Figure 4.3 and Figure 4.4 are calculated for the folded 64-layer (PS/PMMA)¹⁶(PMMA/PS)¹⁶ structure.

It is obvious that, in the case of the 128- layer system, there are enhanced band edge effects and the rotation is suppressed inside the reflection band, both consistent with our measured results shown in Figure 3.3. In the case of folded 64-layer system, there is even greater enhancement at the reflection band central defect caused by the half-wavelength defect in the quarter wavelength stack, which is also consistent with our measured results shown in Figure 3.4. The measured results shown in Figure 3.3 and the simulated results shown in Figure 4.2 differ qualitatively because of the effects of layer thickness variations and spectral averaging.

Generally, the Faraday rotation angle is calculated assuming linearly polarized light input and output (E_x) which neglects ellipticity ($\theta_F = \tan^{-1}(\chi)$). However, in one dimensional photonic crystal system, the ellipticity phenomenon can be significant. This phenomenon arises through multiple differential reflections due to the difference between the right circularly polarized and left circularly polarized refractive indices in each layer. In particular, near and in the reflection band, the ellipticity of the output light is indicated by χ being complex. The relationship between the azimuth angle θ and the ellipticity angle ϵ for the real and imaginary parts of the output field ratios is then given as [34]

$$\text{Re}(\chi) = \frac{\tan \theta (1 - \tan^2 \epsilon)}{1 + \tan^2 \theta \tan^2 \epsilon} \quad (4.5)$$

$$\text{Im}(\chi) = \frac{\tan \epsilon (1 - \tan^2 \theta)}{1 + \tan^2 \theta \tan^2 \epsilon} \quad (4.6)$$

Assuming the input azimuth angle θ to be zero (i.e. linear polarization in x-direction), the transmitted Faraday rotation angle and the ellipticity angle can be written as

$$\theta_F = \frac{1}{2} \tan^{-1} \left(\frac{2 \operatorname{Re}(\chi)}{1 - |\chi|^2} \right) \quad (4.7)$$

$$\epsilon = \frac{1}{2} \sin^{-1} \left(\frac{2 \operatorname{Im}(\chi)}{1 + |\chi|^2} \right) \quad (4.8)$$

The results of Figure 4.2 and Figure 4.4 contain the effects of ellipticity in the output polarization angle as supposed by Eq. (4.8), but do not indicate the amount of ellipticity directly, which we did not measure. Figure 4.1 compares the predicted Faraday rotation spectra with ellipticity included (red line) and without taking into account ellipticity (black line) for our 64-layer folded structure, both based on 4×4 transfer matrix approach. It also shows that the 2×2 approach is more closely aligned to the results obtained when ellipticity is properly included.

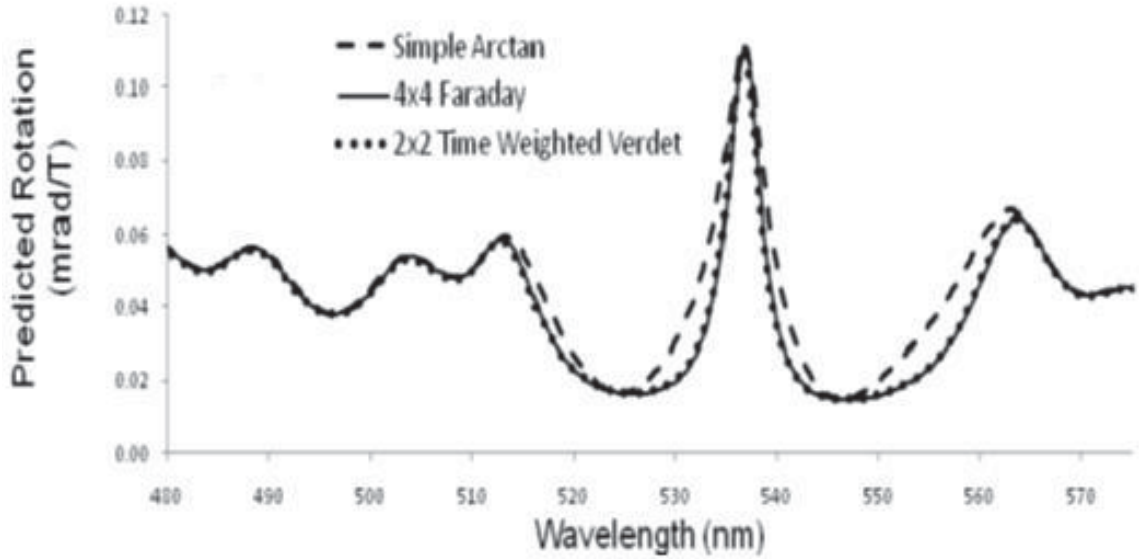


Figure 4.5: Predicted Faraday rotation in terms of ellipticity

[Comparison between predicted Faraday rotation for a folded 64-layer film considering ellipticity (solid line) and without considering ellipticity (dashed line) by using both transfer matrix approaches]

The ellipticity is very small outside the reflection band and both approaches yield same results. However, inside the reflection band, the two approaches deviate due to the accumulated effects of differential reflectivities increasing the ellipticity of the output.

In Figure 4.6, we plot the difference between the models used in Figure 4.4 (i.e. $\theta_{F_{2 \times 2}} - \theta_{F_{4 \times 4}}$). It is obvious that this difference closely follows the predicted ellipticity.

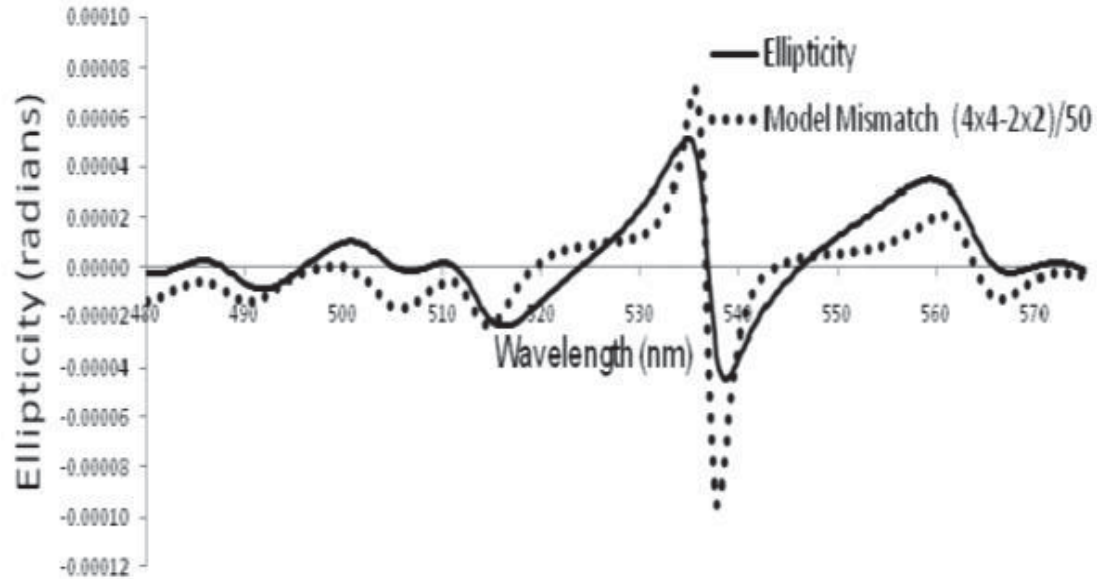


Figure 4.6: Predicted ellipticity angle in terms of scaling

[Comparison between the predicted ellipticity angle for folded 64-layer film (solid line) and the scaled difference between the 4×4 and 2×2 transfer matrix results shown in Figure 4.4 (dotted line)]

4.2: 4×4 TRANSFER MATRIX APPROACH

The preliminary idea for developing our declaration in Eq. (4.2) is the standard 4×4 transfer matrix technique for calculating Faraday effects in multilayers. The implementation of this technique is for both the transmission and Faraday characteristics of purely dielectric multilayers starting from considerations of magnetically-induced circular birefringence (i.e., the differential indices of refraction for left circularly polarized light and right circularly polarized light in the presence of an applied magnetic field) [35]. The energy-weighted group velocity delay was represented operationally by determining the time spent in each component of the medium. The 4×4 transfer matrix approach is realized in Appendix B.

At zero magnetic field, the orthogonal linear polarization states (i.e., E_x and E_y) moving through the non-birefringent material have identical characteristic 2×2 transfer matrices in (E, H) basis of the usual form for multilayer transmission calculations,

$$\mathbf{M} = \begin{bmatrix} \cos\delta & \left(\frac{i\sin\delta}{\eta}\right) \\ i\eta \sin\delta & \cos\delta \end{bmatrix} \quad (4.9)$$

where,

η = complex impedance of the medium at frequency ω

$\delta = nk_0x$ = optical path length measured in vacuum wavelengths of the material in terms of the index of refraction (n) and the vacuum wave-vector (k_0)

To couple these two orthogonal polarization states, the characteristic matrices \mathbf{M} is combined for each layer with the 2×2 coupling matrices \mathbf{C} into a 4×4 transfer matrix $\mathbf{m} = \begin{bmatrix} \mathbf{M} & \mathbf{C} \\ -\mathbf{C} & \mathbf{M} \end{bmatrix}$, where the \mathbf{C} matrix represents the vertical and horizontal optical rotation assuming no absorption or incoherent scattering. For purely dielectric materials, in the limit of small Faraday rotations, \mathbf{C} can be written as

$$\mathbf{C} = VB \begin{bmatrix} -i \sin\delta & \frac{1}{n}(\cos\delta - \frac{\sin\delta}{\delta}) \\ n(\cos\delta + \frac{\sin\delta}{\delta}) & -i \sin\delta \end{bmatrix} \quad (4.10)$$

where,

V = bulk Verdet coefficient for the constituent material

B = applied magnetic field (i.e., 1 Tesla for our experiments and simulations)

Eq. (4.10) can be simplified as

$$\mathbf{C} = \mathbf{C}_p + \mathbf{C}_s \quad (4.11)$$

where,

$$\mathbf{C}_p = VB \begin{bmatrix} -i \sin\delta & \frac{1}{n} \cos\delta \\ n \cos\delta & -i \sin\delta \end{bmatrix} \quad (4.12)$$

$$\mathbf{C}_s = VB \frac{\sin\delta}{\delta} \begin{bmatrix} 0 & -\frac{1}{n} \\ n & 0 \end{bmatrix} \quad (4.13)$$

Thus, the characteristics 4×4 transfer matrix for each layer represents the phase and amplitude changes in that layer as well as the coupling of the left circularly polarized and right circularly polarized refractive indices as a function of applied magnetic field for the constituent materials. Operation of the transfer matrices \mathbf{m} of each kayer on the fields

can be expressed as a 4-dimensional complex vector $\begin{pmatrix} E_x \\ H_y \\ E_y \\ -H_x \end{pmatrix}$ (where, in our case, the

incoming E_y and H_x are assumed to be zero). The ratio of horizontal (E_x) and vertical (E_y) polarization outputs (i.e., $\chi = \frac{E_x}{E_y}$) has a complex value.

The fact that the \mathbf{C}_p and \mathbf{C}_s scale differently with the thickness of the layers indicates that in most situations, the Faraday rotation is dominated by the contributions from the primary part \mathbf{C}_p .

Solving Eq. (4.9) and Eq. (4.13), we get

$$\mathbf{M}^{-1} \mathbf{C}_p = VB \begin{bmatrix} 0 & \frac{1}{n} \\ n & 0 \end{bmatrix} = iVB \{ \partial_\delta \mathbf{M} \} \mathbf{M}^{-1} \quad (4.14)$$

where, the material's intrinsic refractive index dispersion is ignored

The optical transport in the complex medium is the product of the 4×4 transfer matrices \mathbf{m} for each component labeled by 'i' in sequence. In the limit of small Faraday rotations, we need only need to keep terms linear in the V_i and thus have

$$\mathbf{m} = \prod_i \mathbf{m}_i = \begin{bmatrix} \mathbf{M} & \mathbf{C} \\ -\mathbf{C} & \mathbf{M} \end{bmatrix} \quad (4.15)$$

$$\text{Then, } \mathbf{M} = \prod_i \mathbf{M}_i \quad (4.16)$$

$$\mathbf{C}_p = \mathbf{M} \mathbf{S} \quad (4.17)$$

$$\text{where, } \mathbf{S} = \sum_i \mathbf{P}_i^{-1} \mathbf{M}_i^{-1} \mathbf{C}_{pi} \mathbf{P}_i \text{ [for } \mathbf{M} = \mathbf{N}_i \mathbf{M}_i \mathbf{P}_i \text{ for each } i] \quad (4.18)$$

$$\mathbf{N}_i = \prod_{j>1} \mathbf{M}_j \quad (4.19)$$

$$\mathbf{P}_i = \prod_{j<1} \mathbf{M}_j \quad (4.20)$$

The vectors $\mathbf{w}_t = \frac{1}{2} (1, 1)$ and $\mathbf{w}_r = \frac{1}{2} (1, -1)$ are the transmission and reflection propagation eigenstates in the $n = 1$ medium to the left and right of the layered medium. . Thus, taking the ratio of the horizontal transmitted component to the vertical transmitted component, the observed Faraday rotation is

$$\theta_F \sim \arctan(\chi) \sim |\mathbf{w}_t^T \mathbf{M} \mathbf{S} \mathbf{M}^{-1} \mathbf{w}_t| = |iB \sum_i V_i \mathbf{w}_t^T \mathbf{N}_{i+1} \{ \partial_\delta \mathbf{M}_i \} \mathbf{M}_i^{-1} \mathbf{N}_{i+1}^{-1} \mathbf{w}_t| \quad (4.21)$$

where, \mathbf{w}_t^T = transpose vector of \mathbf{w}_t .

This expression can then be related to sum of the energy-weighted time in each layer multiplied by the rotation (per unit time) in that layer. It should be noted that the transmission amplitude is

$$\tau = \frac{1}{\mathbf{w}_t^T \mathbf{M}^{-1} \mathbf{w}_t} \quad (4.22)$$

Eq. (4.22) indicates that the total group velocity delay across the entire multilayer (i.e., ‘ i ’ times the derivative with respect to the wavevector of the phase of the transmission amplitude) given by

$$\partial_{k_0} \phi = \frac{1}{2i} \left[\frac{\partial_{k_0} \tau}{\tau} - \frac{\partial_{k_0} \tau^*}{\tau} \right] = \frac{\tau^2}{2i} \left[\mathbf{w}_t^T (\partial_{k_0} \mathbf{M}^{*-1}) \mathbf{w}_t \mathbf{w}_t^T \mathbf{M}^{-1} \mathbf{w}_t - c.c \right] \quad (4.23)$$

where, $c.c =$ complex conjugate for $\{\mathbf{w}_t^T (\partial_{k_0} \mathbf{M}^{*-1}) \mathbf{w}_t \mathbf{w}_t^T \mathbf{M}^{-1} \mathbf{w}_t\}$.

Here, the multilayer systems we are studying are very close to being parity symmetric, that is,

$$\mathbf{M}^l = \mathbf{TMT} \quad (4.24)$$

$$\text{where, } \mathbf{T} = \begin{bmatrix} -1 & 0 \\ 0 & 1 \end{bmatrix} \quad (4.25)$$

Eq. (4.25) maps outgoing states to ingoing states in the original 2×2 systems.

Since there is no absorption it implies that the power quadratic form \mathbf{P} satisfies

$$\mathbf{P} = \mathbf{M}^T \mathbf{P} \mathbf{M} \quad (4.26)$$

$$\text{where in this } 2 \times 2 \text{ basis, } \mathbf{P} = \begin{bmatrix} 0 & 1 \\ 1 & 1 \end{bmatrix} \quad (4.27)$$

This reflection symmetry of the film implies that

$$\mathbf{M}^l = \mathbf{M}^* \quad (4.28)$$

Eq. (4.28) is true only for the multilayers $(AB)^N(BA)^N$, $(AB)^NA$ or $(AB)^N$ for large N .

Under the even parity and no absorption assumptions, the term $\mathbf{w}_r \mathbf{M}^l \mathbf{w}_t$ is purely imaginary. Then using

$$\mathbf{w}_t \mathbf{w}_t^T + \mathbf{w}_r \mathbf{w}_r^T = \begin{bmatrix} 1 & 0 \\ 0 & 1 \end{bmatrix} \quad (4.29)$$

The total group velocity takes a form

$$\partial_{k_0} \phi = i\tau^2 \mathbf{w}_t^T (\partial_{k_0} \phi \mathbf{M}) \mathbf{M}^l \mathbf{w}_t \quad (4.30)$$

and the expression

$$\mathbf{w}_t^T (\partial_{k_0} \phi \mathbf{M}) \mathbf{M}^l \mathbf{w}_t = \sum_j \mathbf{w}_t^T \mathbf{N}_j n_j l_j (\partial_\delta \mathbf{M}_j) \mathbf{M}_j^{-1} \mathbf{N}_j^{-1} \mathbf{w}_t, \quad (4.31)$$

where, n_j = index of refraction of j^{th} layer

l_j = thickness of j^{th} layer

The term $\mathbf{N}_j^{-1} \tau \mathbf{w}_t$ is the local (E_j, H_j) at that layer's output fact. The $n_j (\partial_\delta \mathbf{M}_j) \mathbf{M}_j^{-1}$ as a quadratic form on that field vector gives one the normalized local energy density in the standing wave and scaled by l_j gives the normalized local circulating energy in the j^{th} component.

For non-absorption assumption, let

$$\mathbf{N}_j = \begin{bmatrix} a & ib \\ ic & d \end{bmatrix} \quad (4.32)$$

where a, b, c, d are real

Since the transport is power conserving,

$$\det(\mathbf{N}_j) = 1 \quad (4.33)$$

Then,

$$E_j = \tau(d \quad ib) \quad (4.34)$$

$$H_j = \tau(a \quad ic) \quad (4.35)$$

$$\mathbf{w}_t^T \mathbf{N}_j n_j l_j (\partial_\delta \mathbf{M}_j) \mathbf{M}_j^{-1} \mathbf{N}_j^{-1} \mathbf{w}_t = n E_j^* E_j + \frac{1}{n} H_j^* H_j \quad (4.36)$$

At this point the connection between the group velocity delay $\partial_{k_0} \phi$ and the Faraday rotation θ_F is straightforward. The derivative $\partial_{k_0} \phi$ is related to the terms making up the Faraday rotation by allocating the total delay into delays in each component proportional to the total energy density in that component. The total delay is given by

$$t_d = \frac{1}{c} \partial_{k_0} \phi \quad (4.37)$$

For simplicity of notation, assume that the system was just $(AB)^N$.

$$\text{Then } t_A = \langle u_A \rangle t_d \quad (4.38)$$

$$t_B = \langle u_B \rangle t_d \quad (4.39)$$

where, t_A = time in material A

t_B = time in material B

“ $\langle \rangle$ ” means normalized in terms total circulating energy $u_A + u_B$

Thus, as described in Eq. (4.2), for the primary part of the Faraday rotation,

$$\frac{\theta_F}{B} = v_A t_A + v_B t_B \quad (4.40)$$

Thus, we derived a connection between the primary part of the Faraday rotation (usually computed in the 4×4 formalism) and the total group delay in a complex linear medium (from the 2×2 problem), assuming no intrinsic media dispersion, no absorption and parity of the medium. We have shown that the local energy of a layer (again, using the 2×2 formalism) represents for what fraction of the delay is spent in that layer. This provides an analytical description of the Faraday rotation in complex media in terms of the rotary power of the individual components and the dispersion created by the multilayer structure itself.

CHAPTER 5: LIMITATIONS OF TRANSFER MATRIX APPROACHES

The two MATLAB programs discussed in Appendix A and Appendix B were also used to study the transmission spectrum and Faraday rotation of 16 layer PS/PMMA. The transmission spectrum and Faraday rotation of 16 layer PS/PMMA that were obtained from the 4×4 transfer matrix approach and the 2×2 transfer matrix approach were compared.

Figure 5.1 shows the transmission of 16-layer PS/PMMA obtained from two different approaches. As expected, both the curves were exactly alike.

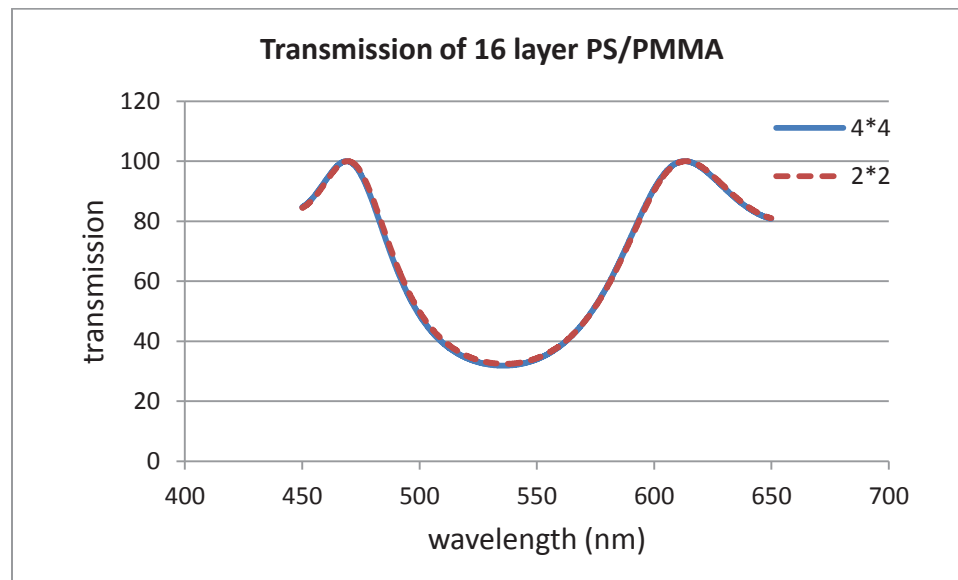


Figure 5.1: Transmission spectrum of 16 layer PS/PMMA

The two transfer matrix approaches showed different results while calculating Faraday rotation. Figure 5.2 compared the rotation obtained from two different approaches when 2nd layer of 16 layered PS/PMMA was considered as special layer. The term special layer was defined in such way that the Verdet value of 2nd layer was

increased by some factor (here, by a factor of 100) while all the Verdet values of other layers were considered to be zero.

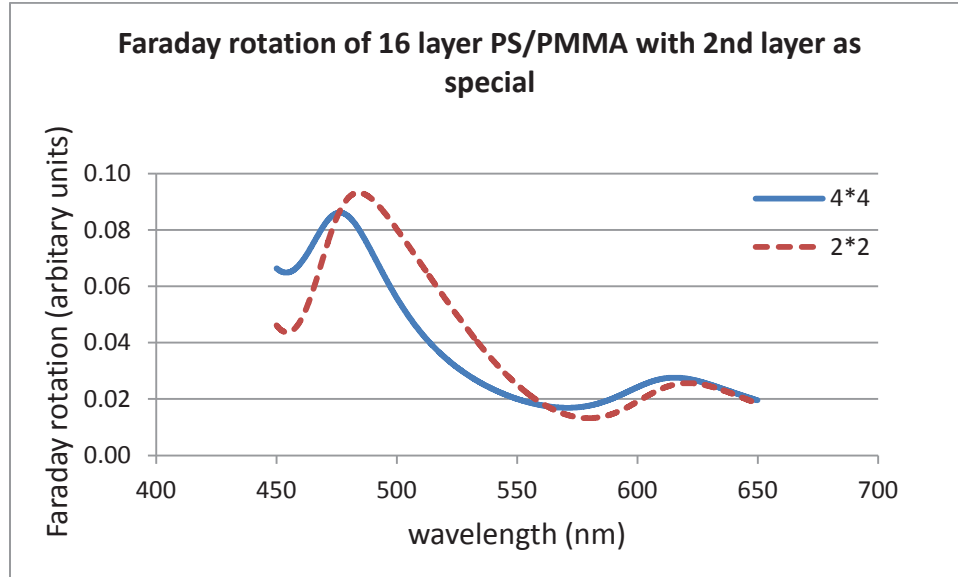


Figure 5.2: Faraday rotation when 2nd layer is considered as special layer

It was obvious from Figure 5.2 that the rotations obtained from two different approaches were not the same. The 2×2 rotation curve represented by the dashed line in the Figure 5.2 had different band. There was also the difference at the band edges for both the curves. This indicated that the two transfer matrix techniques had limitations and that they could not be applied in case of sample with few layers.

The same differences in 4×4 rotation curve and 2×2 rotation curve were seen in 16 layer PS/PMMA when 4th, 6th, 8th, 10th, 12th, 14th and 16th layers were made special layers. The results are shown in Figure 5.3, Figure 5.4, Figure 5.5, Figure 5.6, Figure 5.7, Figure 5.8 and Figure 5.9.

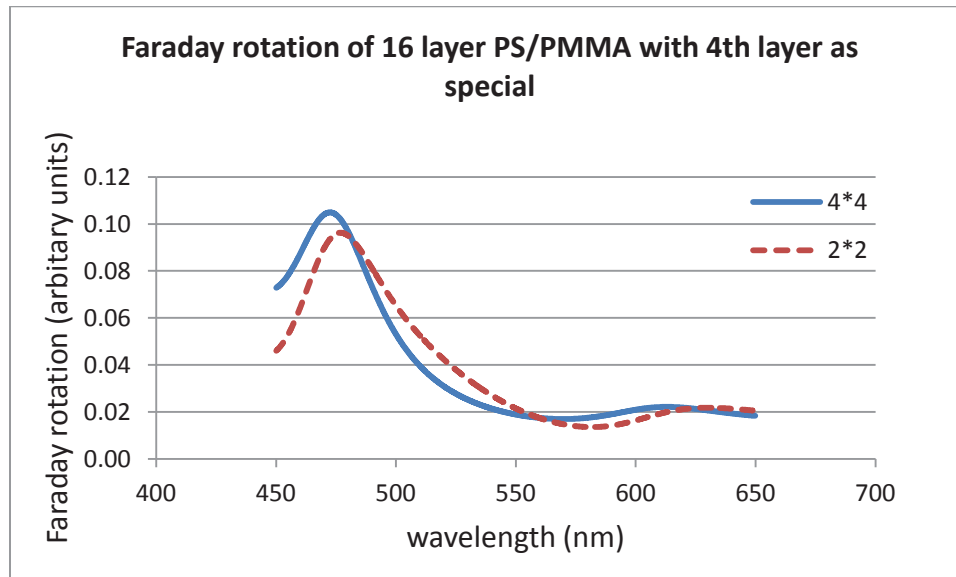


Figure 5.3: Faraday rotation when 4th layer is considered as special layer

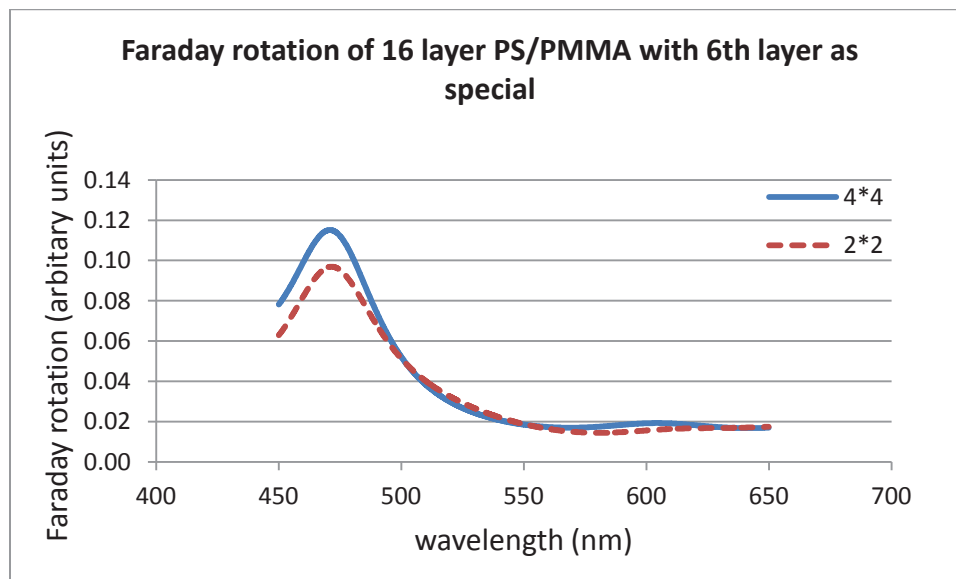


Figure 5.4: Faraday rotation when 6th layer is considered as special layer

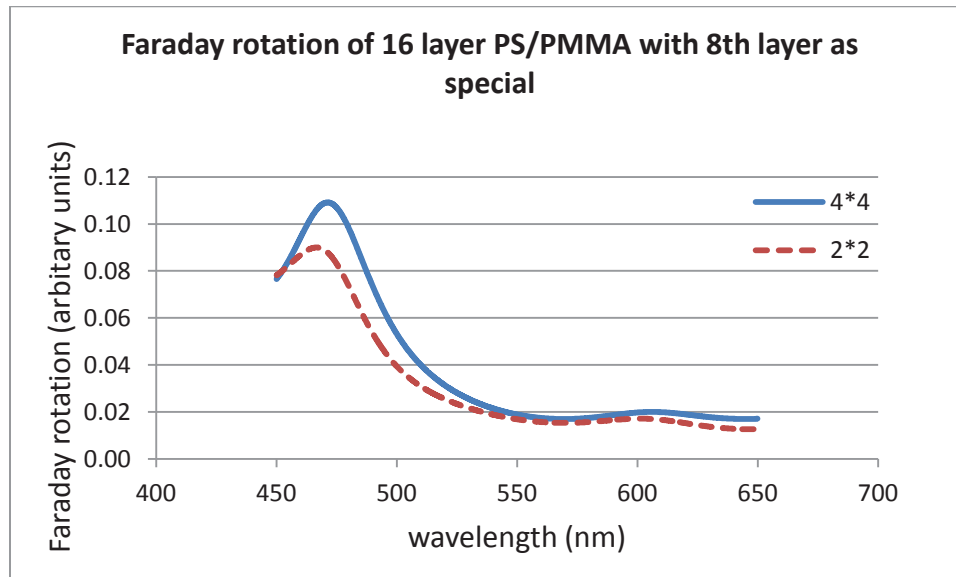


Figure 5.5: Faraday rotation when 8th layer is considered as special layer

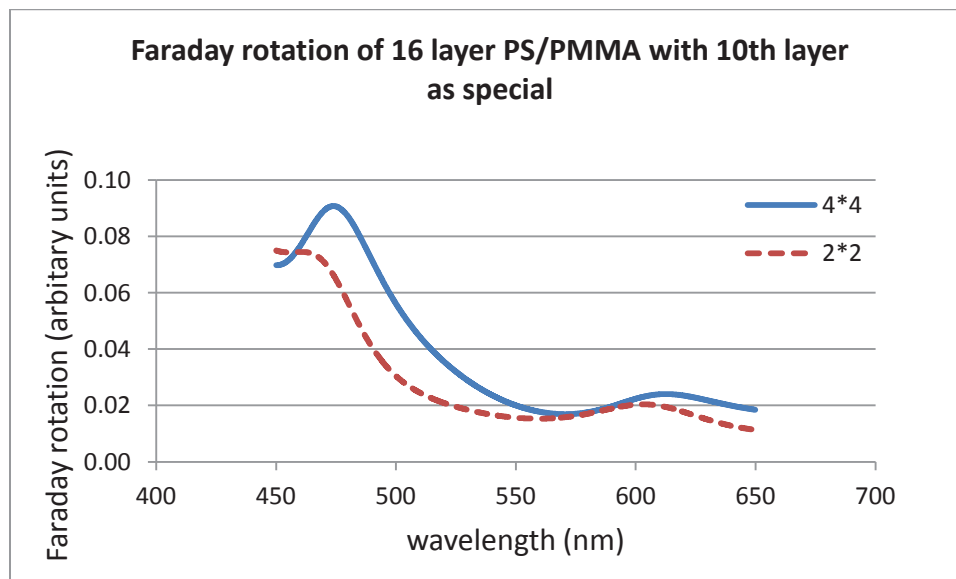


Figure 5.6: Faraday rotation when 10th layer is considered as special layer

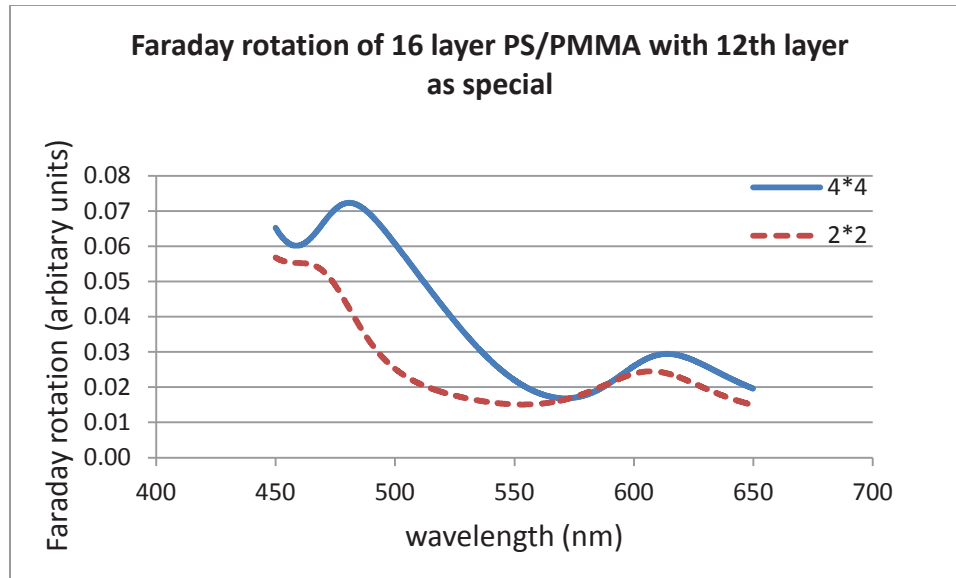


Figure 5.7: Faraday rotation when 12th layer is considered as special layer

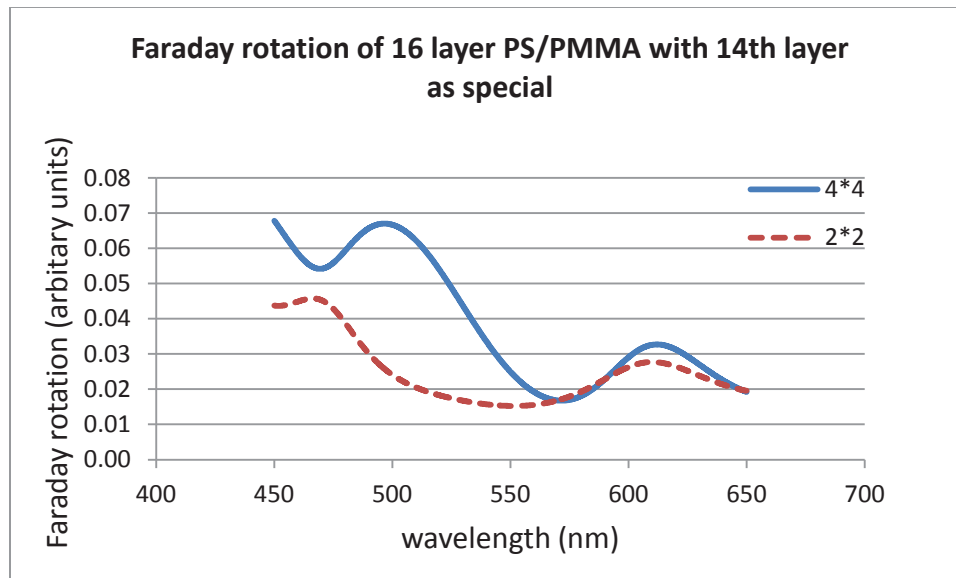


Figure 5.8: Faraday rotation when 14th layer is considered as special layer

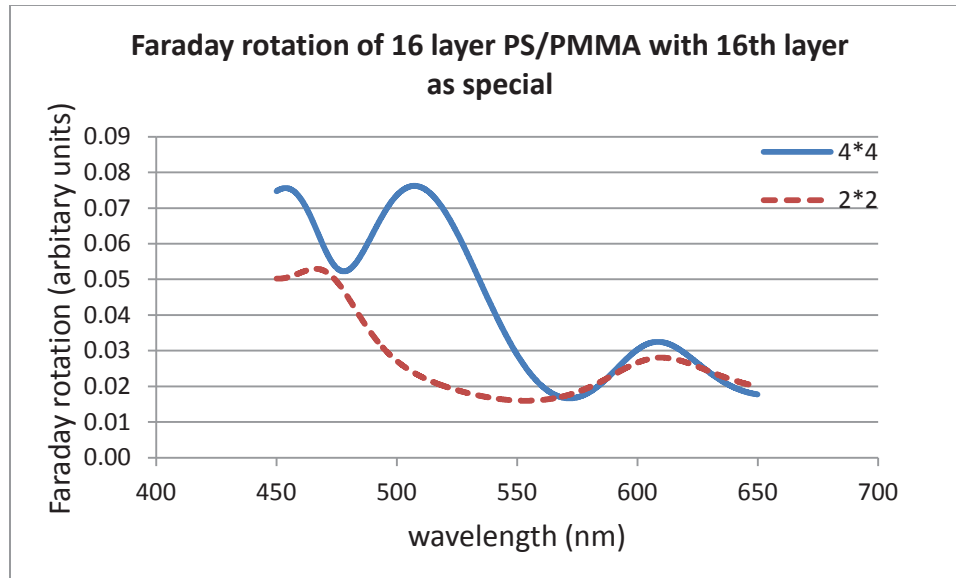


Figure 5.9: Faraday rotation when 16th layer is considered as special layer

Furthermore, we tried to apply the 4×4 and 2×2 transfer matrix techniques in non-symmetric [i.e., $(AB)^n$] 8 layer, 16 layer and 32 layer PS/PMMA multilayer film. The results are shown in Figure 5.10, Figure 5.11 and Figure 5.12. But, the rotations obtained from two different approaches diverged and were not consistent with each other. Thus, it can be concluded the two techniques failed to provide consistency in case of Faraday rotation when the photonic crystals have few numbers of layers.

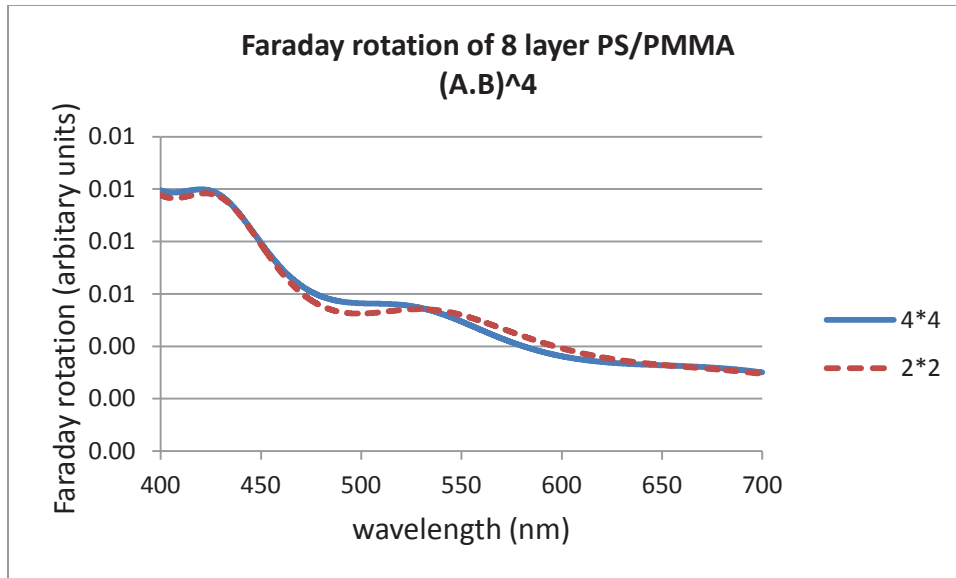


Figure 5.10: Faraday rotation of 8 layer PS/PMMA

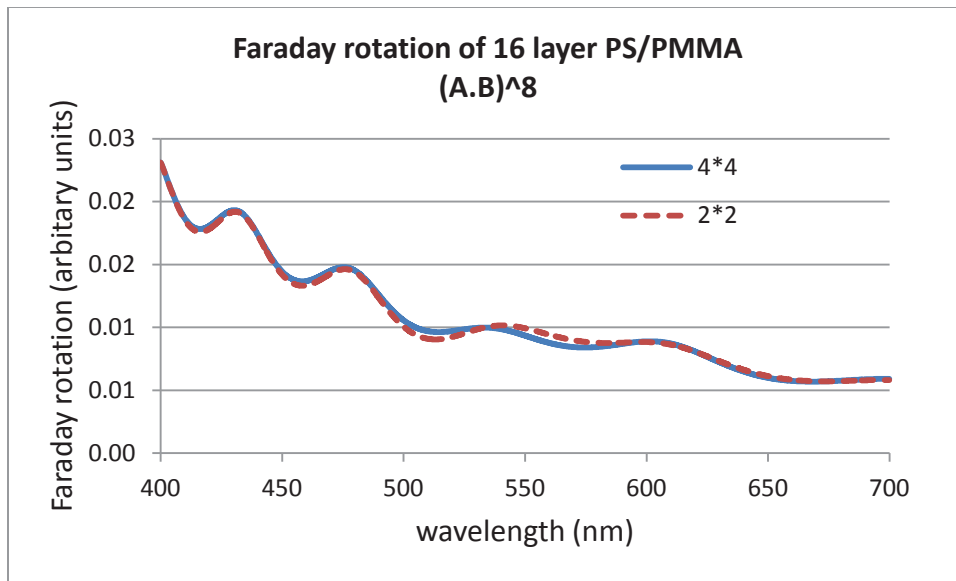


Figure 5.11: Faraday rotation of 16 layer PS/PMMA

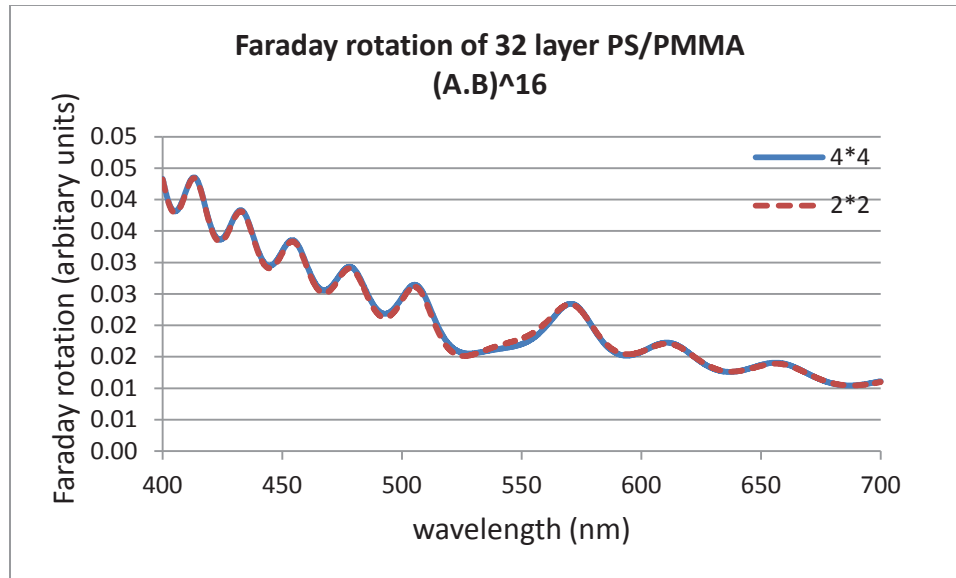


Figure 5.12: Faraday rotation of 32 layer PS/PMMA

CHAPTER 6: CONCLUSION

The Faraday rotation and transmission spectrum of the film both showed oscillations outside of the reflection band, consistent with predictions for a finite multilayer stack. Furthermore, light travelled once through the system at wavelengths well outside the reflection band whereas, at wavelengths near the reflection band or at band defects, light experienced multiple reflections thus increasing the time of transit through the system and relatively increasing the rotation angle. The differences in the group velocity and concentration of the light in different species in the multilayer film caused differences in the band-edge enhancement at short and long wavelengths of the reflection band and defect band. Generally, for a multilayer system having equal alternating thickness layers, the long wavelength band-edge concentrated light in higher refractive index component and the short wavelength band-edge was dominated by the lower refractive index component. However, our experiments showed more band-defect enhancements in the multilayer films having random thickness layers. This can be controlled when systematic defects are included in the structure through the use of folded multilayers discussed earlier. All these cases can be explained by changes in the group velocity associated with band-edges and band defects and that the group velocity delay scales appropriately with the Faraday rotation for these systems and not directly with thickness. Based on this study, we showed that a more relevant equation than Eq (1.2) for Faraday rotation in one-dimensional photonic crystals could be expressed as

$$\theta_F = \int [V(\lambda) v_g] B dt = \int v(\lambda) B dt \quad (5.1)$$

where, $\nu(\lambda)$ is a reduced Verdet constant with the dimensions of angle per magnetic field per second.

To conclude, the magneto-optic rotation caused in the multilayer films composed of alternating layers of two different polymers (i.e. PMMA and PS), was modeled and measured. In order to understand the relationship between Verdet values and the effects of the dispersion of multilayer film, we build up and analyzed a model that illustrated the Faraday rotation in terms of the time spent in each component of the multilayer film. The standard 2×2 transfer matrix technique was used to calculate the total time spent in the system and the relative amount of that time spent in each component of the system. The model confined band-edge and band-defect enhancements of the Faraday rotation and the significant drop in the Faraday rotation in the center of the reflection band.

APPENDICES

APPENDIX A: REALIZATION OF 2×2 TRANSFER MATRIX APPROACHES

In Chapter 4, the 2×2 transfer matrix approaches is discussed. The MATLAB program (written in M-file) used to realize this approach is given in this appendix. The program realizes 2×2 transfer matrix approaches in 128-layer (PS/PMMA)⁶⁴ film to calculate the transmission spectrum and Verdet weighting of Energy/Time in the layers. This verdet weighting data is multiplied with the time calculated from 4×4 approach (i.e., function DelayData (RR)) to obtain Faraday rotation.

MATLAB Code:

```
clear; % Clear workspace in the program

numberdispersion = 1;
ltotal =128; % total layers of PS/PMMA
n1 = 1.49; % Refractive index of PMMA
n2 = 1.585; % Refractive index of PS
nm = 1;
ns = 1;
nd = 1;
d1 = 0.1;
d2 = 0.1;
dd = 0;
abscoeff1 = 0;
abscoeff2 = 0;
abscoeffd = 0;
wlbound1 = 450;
wlbound2 = 650;
wlinc = 10;
sublayers = 10;
numberaverages = 1;

%%%%%%%%%%%%%%%%%%%%%%%%%%%%%%%%%%%%%%%%%%%%%%%%%%%%%%%%%%%%%%%%%%%%%%%%

% Assigning number of points for wavelength
wlength(1:( (wlbound2-wlbound1)*wlinc)+1, 1) =
wlbound1:1/wlinc:wlbound2;

% total wavelength points
```



```

Qjprime = zeros(length(wlength),ltotal*sublayers);
Tprime = zeros(length(wlength),1);
Etotprime = zeros(length(wlength),1);
EtotLprime = zeros(length(wlength),1);
EtotHprime = zeros(length(wlength),1);

%%%%%%%%%%%%%%%%%%%%%%%%%%%%%%%%%%%%%%%%%%%%%%%%%%%%%%%%%%%%%%%%%%%%%%%%

% Define matrix which gives the weighting
Verdetmatrix = zeros(length(wlength),ltotal);

%Read and input refractive indices from a file 'indices.txt'
path(path, 'C:\Users\bshakya\Desktop');
FileName2 = 'indices.txt';
Refraction = dlmread(FileName2);
Refraction(ltotal+1) = ns;

%%%%%%%%%%%%%%%%%%%%%%%%%%%%%%%%%%%%%%%%%%%%%%%%%%%%%%%%%%%%%%%%%%%%%%%%

% Tell the program which is first, L or H.
% L=Low refractive index, and H=High refractive index
% refractive index
    if Refraction(1) > Refraction(2)
        H = 1;
        L = 2;
    elseif Refraction(2) > Refraction(1)
        H = 2;
        L = 1;
    end

Refractionwavelength = zeros(length(wlength), ltotal+1);
    for wl = 1:length(wlength);
        for layer = 1:ltotal+1
            Refractionwavelength(wl,layer) = Refraction(layer,1);
        end
    end
vgroup = zeros(length(wlength), 2);
for layer = 1:ltotal
    for wl = 1:length(wlength)
        if Refractionwavelength(wl,layer) ==1.49;
            Refractionwavelength(wl,layer) = sqrt(2.185+
                1.268*10^4/wlength(wl,1)^2);
            vgroup(wl,L) = 1/Refractionwavelength(wl,layer)*
                (1-1.268*10^4/wlength(wl,1)^2/
                    (Refractionwavelength(wl,layer))^2);

            elseif Refractionwavelength(wl,layer) ==1.585;
                Refractionwavelength(wl,layer) = sqrt(2.440+
                    3.121*10^4/wlength(wl,1)^2);
                vgroup(wl,H) = 1/Refractionwavelength(wl,layer)*
                    (1-3.121*10^4/wlength(wl,1)^2/

```

```

                                (Refractionwavelength(wl,layer))^2);
                                end
                                end
                                end

////////////////////////////////////

stdev = 0;
seed = 65*numberaverages;
randn('seed',seed);
tvar = stdev*randn([(ltotal+1) 1])+1;

% Start of first 'While' loop
while numberaverages<=numberdispersion
clc;
% Read and input thicknesses from a file 'newrandlayer1_6.txt'
path(path,'C:\Users\bshakya\Desktop');
FileName = 'newrandlayer1_6.txt';
Thickness = dlmread(FileName)*10^-3;

Thickness1 = zeros(ltotal,1);
lnumb = 1;
% Start of second 'While' loop
while lnumb<(ltotal+1)
    Thickness1(lnumb,1)= Thickness(lnumb,1)*
    tvar(lnumb,1);
    lnumb=(lnumb+1);
end
% End of second 'While' loop

////////////////////////////////////

    Thickness = Thickness1;

absco = zeros(ltotal+1,1);
for row1 = 1:2:(ltotal-1)
    absco(row1) = abscoeff1;
end

for row2 = 2:2:(ltotal)
    absco(row2) = abscoeff2;
end

    absco(ltotal+1) = 0;
% n+ik
complexrefraction = zeros(length(wlength), ltotal+1);
polarization = zeros(length(wlength), ltotal+1);
del = zeros(length(wlength), ltotal+1);
for layer = 1:ltotal+1
    for wl = 1:length(wlength)

```

```

        complexrefraction(wl,layer) =
        Refractionwavelength(wl,layer)
        - i*((wlength(wl)*(10^-7)*absco(layer))/(4*pi));
        polarization(wl,layer)=
        complexrefraction(wl,layer);
        del(wl,layer) =
        (2*pi*complexrefraction(wl,layer))/
        (wlength(wl)*(10^(-3)));
    end
end

dell = zeros(length(wlength), ltotal);
for layer = 1:ltotal
    for wl = 1:length(wlength)
        dell(wl,layer) = del(wl,layer)*Thickness(layer);
    end
end

%%%%%%%%%%%%%%%%%%%%%%%%%%%%%%%%%%%%%%%%%%%%%%%%%%%%%%%%%%%%%%%%%%%%%%%%

% Define rjk &tjk Fresnel complex reflection & transmission
coefficients
rjk = zeros(length(wlength), ltotal);
tjk = zeros(length(wlength), ltotal);
for j = 1:ltotal
    for wl = 1:length(wlength)

        rjk(wl,j)=(complexrefraction(wl,j)-
        complexrefraction(wl,j+1))/
        (complexrefraction(wl,j)+complexrefraction(wl,j+1));
        tjk(wl,j)=(2*complexrefraction(wl,j))/
        (complexrefraction(wl,j)+complexrefraction(wl,j+1));
    end
end
rmedk = zeros(length(wlength), 1);
tmedk = zeros(length(wlength), 1);
for wl = 1:length(wlength)
    rmedk(wl) = (nm-complexrefraction(wl,1))/
    (nm+complexrefraction(wl,1));
    tmedk(wl) = (2*nm)/(nm+complexrefraction(wl,1));
end

%%%%%%%%%%%%%%%%%%%%%%%%%%%%%%%%%%%%%%%%%%%%%%%%%%%%%%%%%%%%%%%%%%%%%%%%

% Defining Interfjk and Lpropj as propagation matrices
Interfjk = cell(length(wlength),ltotal);
Lpropj = cell(length(wlength),ltotal);
for layer = 1:ltotal
    for wl = 1:length(wlength)
        Interfjk(wl,layer)={[1/tjk(wl,layer)
        rjk(wl,layer)/tjk(wl,layer);
        rjk(wl,layer)/tjk(wl,layer) 1/tjk(wl,layer) ]};
    end
end

```

```

        Lpropj(wl,layer)={ [exp(-i*dell(wl,layer))  0;
                          0  exp(i*dell(wl,layer)) ]};
    end
end

Imed = cell(length(wlength), 1);
for wl = 1:length(wlength)
    Imed(wl) = {[1/tmedk(wl)  rmedk(wl)/tmedk(wl);
                rmedk(wl)/tmedk(wl)  1/tmedk(wl) ]};
end

Matr = cell(length(wlength),ltotal);
M2 = cell(length(wlength),1);
Mstart = cell(length(wlength),1);

for wl = 1:length(wlength)
    for layer = 2:ltotal

        Matr{wl,layer}=(Interfjk{wl,layer}*Lpropj{wl,layer});
    end
    Matr{wl,1} = Imed{wl}*Lpropj{wl,1};
    Mstart{wl,1} = Interfjk{wl,ltotal};
    for layer = ltotal:-1:1
        M2{wl,1} = (Matr{wl,layer}*Mstart{wl,1});
        Mstart{wl,1} = M2{wl,1};
    end
end

end

PbM2 = cell(length(wlength),ltotal);
PfM2 = cell(length(wlength),ltotal-1);
Sji1 = cell(length(wlength),ltotal);
Sji2 = cell(length(wlength),ltotal);
for wl = 1:length(wlength)
    for leftlayer = ltotal:-1:2
        Mstart{wl,1} = Interfjk{wl,leftlayer-1};
        for layer = leftlayer-1:-1:1
            PbM2{wl,leftlayer} =
                Matr{wl,layer}*Mstart{wl,1};
            Mstart{wl,1} = PbM2{wl,leftlayer};
        end
        Sji1{wl,leftlayer} = PbM2{wl,leftlayer};
    end
    Sji1{wl,1} = Imed{wl};

    for rightlayer = 1:ltotal-1
        Mstart{wl,1} = Interfjk{wl,ltotal};
        for layer = ltotal:-1:rightlayer+1
            PfM2{wl,rightlayer} =
                Matr{wl,layer}*Mstart{wl,1};

```

```

        Mstart{wl,1} = Pfm2{wl,rightlayer};
    end
    Sji2{wl,rightlayer} = Pfm2{wl,rightlayer};
end
Sji2{wl,ltotal} = Interfjk{wl,ltotal};
end

for wl = 1:length(wlength)
M2{wl,1} = Sji1{wl,1}*Lpropj{wl,1}*Sji2{wl,1};
End

%%%%%%%%%%%%%%%%%%%%%%%%%%%%%%%%%%%%%%%%%%%%%%%%%%%%%%%%%%%%%%%%%%%%%%%%

% Divide each layer into sublayers
Enum = zeros(length(wlength),sublayers*ltotal);
Edenom = zeros(length(wlength),sublayers*ltotal);
E = zeros(length(wlength),sublayers*(ltotal-1)+1);
Q = zeros(length(wlength),sublayers*(ltotal-1)+1);
for wl = 1:length(wlength)
    for j = 1:ltotal
        % Add one more
        for incr = 1:sublayers
            Enum(wl,sublayers*(j-1)+incr)=Sji2{wl,j}(1)*
                exp(-i*del(wl,j)*(Thickness(j)*
                    (1-incr/sublayers)))+Sji2{wl,j}(2)*
                exp(i*del(wl,j)*(Thickness(j)*
                    (1-incr/sublayers)));

            Edenom(wl,sublayers*(j-1)+incr) =
                Sji1{wl,j}(1)*Sji2{wl,j}(1)*
                exp(-i*del(wl,j)*(Thickness(j)))+
                Sji1{wl,j}(3)*Sji2{wl,j}(2)*
                exp(i*del(wl,j)*(Thickness(j)));

            E(wl,sublayers*(j-1)+incr) =
                Enum(wl,sublayers*(j-1)+incr)./
                Edenom(wl,sublayers*(j-1)+incr);

            Q(wl,sublayers*(j-1)+incr) =
                (Refractionwavelength(wl,j)^2).*
                (E(wl,sublayers*(j-1)+incr)).*
                conj(E(wl,sublayers*(j-1)+incr)))* Thickness(j);
        end
    end
end

%%%%%%%%%%%%%%%%%%%%%%%%%%%%%%%%%%%%%%%%%%%%%%%%%%%%%%%%%%%%%%%%%%%%%%%%

% For partial view of layers
startlayer = 1;
endlayer = ltotal;

```

```

    Qj = zeros(length(wlength), (endlayer-
startlayer+1)*sublayers);

for z7 = (startlayer-1)*sublayers+1:endlayer*sublayers
    for wl = 1:length(wlength)
        Qj(wl,z7-((startlayer-1)*sublayers)) = Q(wl,z7);
    end
end

Etot = zeros(1,length(wlength));
EtotL = zeros(1,length(wlength));
EtotH = zeros(1,length(wlength));

%%%%%%%%%%%%%%%%%%%%%%%%%%%%%%%%%%%%%%%%%%%%%%%%%%%%%%%%%%%%%%%%%%%%%%%%

for wl = 1:length(wlength)
%start
    Etot(1, wl) = sum(Qj(wl,1:endlayer*sublayers));
    numberHlayers = 1;

    if H<L
        while numberHlayers <=ltotal
            EtotL(1, wl) = sum(Qj(wl, numberHlayers*sublayers +
1:numberHlayers*sublayers+sublayers)) + EtotL(1, wl);

            EtotH(1, wl) = sum(Qj(wl, (numberHlayers-1)*sublayers
+ 1:numberHlayers*sublayers)) + EtotH(1, wl);

            numberHlayers = numberHlayers+2;
        end
    end
    if L<H
        while numberHlayers <=ltotal
            EtotH(1, wl) = sum(Qj(wl, numberHlayers*sublayers +
1:numberHlayers*sublayers+sublayers)) + EtotH(1, wl);

            EtotL(1, wl) = sum(Qj(wl, (numberHlayers-1)*sublayers
+ 1:numberHlayers*sublayers)) + EtotL(1, wl);

            numberHlayers = numberHlayers+2;
        end
    end
end
% end

%%%%%%%%%%%%%%%%%%%%%%%%%%%%%%%%%%%%%%%%%%%%%%%%%%%%%%%%%%%%%%%%%%%%%%%%

transmission = zeros(length(wlength), 1);
for wl = 1:length(wlength)
    transmission(wl, 1) = 1/M2{wl, 1}(1);
    PhaseD(wl, 1) = angle(transmission(wl, 1));
end

```

```

end

%%%%%%%%%%%%%%%%%%%%%%%%%%%%%%%%%%%%%%%%%%%%%%%%%%%%%%%%%%%%%%%%%%%%%%%%

% start of unwinding the phase
for ii=1:length(wlength)-1
    if (PhaseD(ii+1)-PhaseD(ii))>3
        for jj=ii+1:length(wlength)
            PhaseD(jj)=PhaseD(jj)-2*pi;
        end
    end
end
end
% end of unwinding the phase

%%%%%%%%%%%%%%%%%%%%%%%%%%%%%%%%%%%%%%%%%%%%%%%%%%%%%%%%%%%%%%%%%%%%%%%%

T = zeros(length(wlength),1);
for wl = 1:length(wlength)
    T(wl,1) = (ns/(nm))*((abs(transmission(wl,1)))^2)*100;
end

%%%%%%%%%%%%%%%%%%%%%%%%%%%%%%%%%%%%%%%%%%%%%%%%%%%%%%%%%%%%%%%%%%%%%%%%

for wl = 1:length(wlength) % start
    Etotprime(wl,1) = Etotprime(wl,1) + Etot(1,wl);
    EtotLprime(wl,1) = EtotLprime(wl,1) +
        EtotL(1,wl);

    EtotHprime(wl,1) = EtotHprime(wl,1) +
        EtotH(1,wl);

    Tprime(wl,1) = Tprime(wl,1) + T(wl);

    for layers = 1:ltotal*sublayers
        Qjprime(wl,layers) = Qjprime(wl,layers) +
            Qj(wl,layers);
    end
end % end

%%%%%%%%%%%%%%%%%%%%%%%%%%%%%%%%%%%%%%%%%%%%%%%%%%%%%%%%%%%%%%%%%%%%%%%%

numberaverages = numberaverages + 1;

end
% End of first 'While' loop

%%%%%%%%%%%%%%%%%%%%%%%%%%%%%%%%%%%%%%%%%%%%%%%%%%%%%%%%%%%%%%%%%%%%%%%%

% Define matrix that calculates the total energy
EtotMike = zeros(length(wlength),1);

```

```

% Start of 'for' loop for splayer
for splayer=1:4
clc;

% Start of for loop for length(wlength) i.e total wavelength
for wl = 1:length(wlength)
    clc;
    Tprime(wl,1) = Tprime(wl,1)/numberdispersion;
    Etotprime(wl,1) = (EtotLprime(wl,1) +
    EtotHprime(wl,1))/numberdispersion;

% Start of 'for' loop for ltotal i.e total layers
for layer=1:ltotal
    clc;

    % Start of second 'if' loop
    if mod(layer,2)==1 % odd splayer
        Verdetmatrix(wl,ltotal)=
        2.27*10^6/(wlength(wl,1)^2)+
        2.21*10^11/(wlength(wl,1)^4);

        if layer==splayer
            Verdetmatrix(wl,ltotal)=
            50*(2.27*10^6/(wlength(wl,1)^2)+
            2.21*10^11/(wlength(wl,1)^4));
        end

        EtotLprime(wl,1)=(Verdetmatrix(wl,ltotal)*vgroup(wl,L)
        * EtotLprime(wl,1))/numberdispersion;

        elseif mod(layer,2)==0 % even splayer

            Verdetmatrix(wl,ltotal)=7.397*10^5/(wlength(wl,1)
            ^2)+ 1.1*10^11/(wlength(wl,1)^4);

            if layer==splayer
                Verdetmatrix(wl,ltotal)=50*(7.397*10^5/(wlength(wl,1)
                ^2)+ 1.1*10^11/(wlength(wl,1)^4));
            end

            EtotHprime(wl,1) = (Verdetmatrix(wl,H)*vgroup(wl,H)*
            EtotHprime(wl,1))/numberdispersion;
        end

        % End of second 'if' loop
        EtotMike(wl,1) = (EtotLprime(wl,1)+EtotHprime(wl,1))/
        (Etotprime(wl,1));

    end

% End of 'for' loop for ltotal i.e total layers

```



```

    for layers = 1:ltotal*sublayers                % start
        Qjprime(wl,layers) =
            Qjprime(wl,layers)/numberdispersion;
    end                                            % end

end

% End of 'for' loop for length(wlength) i.e total wavelength

%%%%%%%%%%%%%%%%%%%%%%%%%%%%%%%%%%%%%%%%%%%%%%%%%%%%%%%%%%%%%%%%%%%%%%%%

% Transmission Plot
figure('Name','Transmittance', 'Numbertitle', 'off')
hold on;
plot(wlength(1:length(T)), T(:), 'r'),
xlabel('Wavelength (nm)'),
ylabel('Wavelength (nm)'),title('Transmission');
grid on

saveas(gcf,'Transmission_with_MCC_Layers_HL_128_with_dispersion.jpg','jpg')

% Weighted Total Energy (Crescimanno) vs Wavelength Plot
figure('Name','Total Energy
vs.Wavelength', 'Numbertitle','off');
plot(wlbound1:1/wlinc:wlbound2, (EtotMike(:))),
xlabel('Wavelength (nm)'),
ylabel(splayer);
title('Photon Localization Weighted by Local Verdets')
grid on

saveas(gcf,'Energy_of_L_and_H_layers_HLLH_32_32_funcnt_lambda_Verdets_weighted_n^2_cresc.jpg', 'jpg')

% Data is as follows:
% column 1, wavelength:
% column 2, Transmission:
% column 3, unweighted energy:
% column 4, weighted energy in layers (by Verdet)
impdata = zeros(length(wlength),5);
for k = 1:length(wlength)
    impdata(k,1) = wlength(k,1);
    impdata(k,2) = Tprime(k,1);
    impdata(k,3) = (Etotprime(k,1))/(ltotal*sublayers);
    impdata(k,4) = (EtotLprime(k,1) +
        EtotHprime(k,1))/(ltotal*sublayers);
    impdata(k,5) = EtotMike(k,1);
end
dlmwrite('LH_128_Rand_1_6.txt', impdata, '\t')

end
% End of 'for' loop for splayer

```

APPENDIX B: REALIZATION OF 4×4 TRANSFER MATRIX APPROACHES

In Chapter 4, the 4×4 transfer matrix approaches is discussed. The MATLAB program (written in M-file) used to realize this approach is given in this appendix. The program realizes the 4×4 transfer matrix approaches in 128-layer (PS/PMMA)⁶⁴ film to calculate the transmission and Faraday rotation. The program performs matrix multiplication using loop commands like for, while, if, else and ifelse.

MATLAB Code:

```
clear; % Clear workspace in the program
nLayer=128; %layer number of sample

% Assigning layer thickness of A (PMMA only)
dA=10^-6*
[4.35E-02; 8.7E-02; 8.7E-02; 8.7E-02; 8.7E-02; 8.7E-02; 8.7E-02;
8.7E-02; 8.7E-02; 8.7E-02; 8.7E-02; 8.7E-02; 8.7E-02; 8.7E-02;
8.7E-02; 8.7E-02; 8.7E-02; 8.7E-02; 8.7E-02; 8.7E-02; 8.7E-02;
8.7E-02; 8.7E-02; 8.7E-02; 8.7E-02; 8.7E-02; 8.7E-02; 8.7E-02;
8.7E-02; 8.7E-02; 8.7E-02; 8.7E-02; 8.7E-02; 8.7E-02; 8.7E-02;
8.7E-02; 8.7E-02; 8.7E-02; 8.7E-02; 8.7E-02; 8.7E-02; 8.7E-02;
8.7E-02; 8.7E-02; 8.7E-02; 8.7E-02; 8.7E-02; 8.7E-02; 8.7E-02;
8.7E-02; 8.7E-02; 8.7E-02; 8.7E-02; 8.7E-02; 8.7E-02; 8.7E-02;
8.7E-02; 8.7E-02; 8.7E-02; 8.7E-02; 8.7E-02; 8.7E-02; 8.7E-02;
8.7E-02; 8.7E-02; 8.7E-02; 8.7E-02; 8.7E-02; 8.7E-02; 8.7E-02;
8.7E-02; 8.7E-02; 8.7E-02; 8.7E-02; 8.7E-02; 8.7E-02; 8.7E-02;
8.7E-02; 8.7E-02; 8.7E-02; 8.7E-02; 8.7E-02; 8.7E-02; 8.7E-02;
8.7E-02; 8.7E-02; 8.7E-02; 8.7E-02; 8.7E-02; 8.7E-02; 8.7E-02;
2.175E-02; 2.175E-02;];

%%%%%%%%%%%%%%%%%%%%%%%%%%%%%%%%%%%%%%%%%%%%%%%%%%%%%%%%%%%%%%%%%%%%%%%%

% start of seed for-loop
for seed =5:5 % seed variable assigned
    stdev = 0;
    randn('seed',seed);
```

```

tvar = stdev*randn([(nLayer+1) 1])+1;
dA1 = zeros(nLayer,1);
lnumb = 1;
while lnumb<(nLayer+1)
    dA1(lnumb,1)= dA(lnumb,1)* tvar(lnumb,1);
    lnumb=(lnumb+1);
end

dA = dA1;

dB=dA; % layer thickness of B (PS only)

%%%%%%%%%%%%%%%%%%%%%%%%%%%%%%%%%%%%%%%%%%%%%%%%%%%%%%%%%%%%%%%%%%%%%%%%

StartLamda=400*10^-9; % start wavelength
EndLamda=500*10^-9; % end wavelength
WavelengthStep=0.025*10^-9; % calculation resolution

% starting overwrite NA and NB (using PS and PMMA)
% index of A: PMMA
% NA=1.49;
% index of B: PS
% NB=1.58;
NOB=2.440;
C1B=3.121*10^-14;

NOA=2.185;
C1A=1.268*10^-14;

ALayerA=7.397*10^5;
ALayerB=1.1*10^11;
BLayerA=2.27*10^6;
BLayerB=2.21*10^11;

% off-diagonal dielectric constant of A at 525nm
e2A0=1;

% off-diagonal dielectric constant of B at 525nm
e2B0=1;

% ending overwrite NA and NB

%%%%%%%%%%%%%%%%%%%%%%%%%%%%%%%%%%%%%%%%%%%%%%%%%%%%%%%%%%%%%%%%%%%%%%%%

TransferN=zeros(4,4); % record the transfer matrix

% number of wavelength points
WaveRes=int16((EndLamda-StartLamda)/WavelengthStep);

LamdaRecord=zeros(1,WaveRes); %record all wavelength
TransData=zeros(1,WaveRes); % tranission data array
RotationData=zeros(1,WaveRes); % rotation data array

```

```

VerdetData=zeros(1,WaveRes); % verdet constant data array
PhaseData=zeros(1,WaveRes); % Phase
EllipData=zeros(1,WaveRes); % Ellipticity
DelayData=zeros(1,WaveRes);
RotationByDelay=zeros(1,WaveRes);

%%%%%%%%%%%%%%%%%%%%%%%%%%%%%%%%%%%%%%%%%%%%%%%%%%%%%%%%%%%%%%%%%%%%%%%%

Lamda=StartLamda; % temporary lamda(for calculation use)
counter=1 % calculation incresement index, for wavelength

while Lamda-EndLamda<0

    % overwrite here
    NA=sqrt(N0A+C1A/(Lamda^2));
    NB=sqrt(N0B+C1B/(Lamda^2));

    e2A=e2A0*Lamda*(ALayerA/(Lamda*10^9)^2
                +ALayerB/(Lamda*10^9)^4)/2;

    e2B=e2B0*Lamda*(BLayerA/(Lamda*10^9)^2
                +BLayerB/(Lamda*10^9)^4)/2;
    % end of overwrite
    TransferN=eye(4,4);
    TransferN1=zeros(4,4);

%%%%%%%%%%%%%%%%%%%%%%%%%%%%%%%%%%%%%%%%%%%%%%%%%%%%%%%%%%%%%%%%%%%%%%%%

for Layer=1:nLayer

    if mod(Layer,2)==1 % odd layer
        e1=NA*NA;e2=e2A;ep=e1+e2;en=e1-e2;
        dn=2.0*pi*dA(Layer)*sqrt(en)/Lamda;
        dp=2.0*pi*dA(Layer)*sqrt(ep)/Lamda;

        M=[0.5*(cos(dn)+cos(dp)),
            -0.5*i*(cos(dn)-cos(dp)),
            0.5*(1*sin(dn)/sqrt(en)+sin(dp)/sqrt(ep)),
            0.5*i*(sin(dn)/sqrt(en)+sin(dp)/sqrt(ep));
            0.5*i*(cos(dn)cos(dp)),0.5*(cos(dn)+cos(dp)),
            -0.5*i*(sin(dn)/sqrt(en)+sin(dp)/sqrt(ep)),
            0.5*(-1*sin(dn)/sqrt(en)+sin(dp)/sqrt(ep));
            0.5*(sin(dn)*sqrt(en)-sin(dp)*sqrt(ep)),
            -0.5*i*(sin(dn)*sqrt(en)+sin(dp)*sqrt(ep)),
            0.5*(cos(dn)+cos(dp)),
            -0.5*i*(cos(dn)-cos(dp));
            0.5*i*(sin(dn)*sqrt(en)+sin(dp)*sqrt(ep)),
            0.5*(sin(dn)*sqrt(en)-sin(dp)*sqrt(ep)),
            0.5*i*(cos(dn)-cos(dp)),
            0.5*(cos(dn)+cos(dp))];
    end
end

```

```

elseif mod(Layer,2)==0 % even layer
    e1=NB*NB;e2=e2B; ep=e1+e2;en=e1-e2;
    dn=2.0*pi*dB(Layer)*sqrt(en)/Lamda;
    dp=2.0*pi*dB(Layer)*sqrt(ep)/Lamda;

    M=[0.5*(cos(dn)+cos(dp)),
        -0.5*i*(cos(dn)-cos(dp)),
        0.5*( -
        1*sin(dn)/sqrt(en)+sin(dp)/sqrt(ep)),
        0.5*i*(sin(dn)/sqrt(en)+sin(dp)/sqrt(ep));
        0.5*i*(cos(dn)-cos(dp)),
        0.5*(cos(dn)+cos(dp)),
        -0.5*i*(sin(dn)/sqrt(en)+sin(dp)/sqrt(ep)),
        0.5*(-1*sin(dn)/sqrt(en)+sin(dp)/sqrt(ep));
        0.5*(sin(dn)*sqrt(en)-sin(dp)*sqrt(ep)),
        -0.5*i*(sin(dn)*sqrt(en)+sin(dp)*sqrt(ep)),
        0.5*(cos(dn)+cos(dp)),
        -0.5*i*(cos(dn)-cos(dp));
        0.5*i*(sin(dn)*sqrt(en)+sin(dp)*sqrt(ep)),
        0.5*(sin(dn)*sqrt(en)-sin(dp)*sqrt(ep)),
        0.5*i*(cos(dn)-cos(dp)),
        0.5*(cos(dn)+cos(dp))];

    end;

    TransferN=M*TransferN;
end % end of for loop (Layer=1:nLayer)

%%%%%%%%%%%%%%%%%%%%%%%%%%%%%%%%%%%%%%%%%%%%%%%%%%%%%%%%%%%%%%%%%%%%%%%%

% coupling eqns expressed in terms of transfer matrix elements
F1=TransferN(1,1)+TransferN(1,4);
F7=TransferN(2,1)+TransferN(2,4);
F10=TransferN(3,1)+TransferN(3,4);
F4=TransferN(4,1)+TransferN(4,4);
F2=TransferN(1,1)-TransferN(1,4);
F8=TransferN(2,1)-TransferN(2,4);
F11=TransferN(3,1)-TransferN(3,4);
F5=TransferN(4,1)-TransferN(4,4);
F3=TransferN(1,2)+TransferN(1,3);
F9=TransferN(2,2)+TransferN(2,3);
F12=TransferN(3,2)+TransferN(3,3);
F6=TransferN(4,2)+TransferN(4,3);

G1=F2-F5;
G2=F3-F6;
G3=F4-F1;
G4=F8+F11;
G5=F9+F12;
G6=-1*(F7+F10);

del=G1*G5-G2*G4;

```

```

% back reflection X and Y, i.e. C1, C2,
C1=(G3*G5-G2*G6)/del;
C2=(G1*G6-G3*G4)/del;

% transmission X and Y, i.e. C3, and C4
C3=(F2*C1+F3*C2)+F1;
C4=(F8*C1+F9*C2)+F7;

LamdaRecord(1,counter)=Lamda*(10^9);
TransData(counter)=(abs(C3))^2+(abs(C4))^2;
ki=C4/C3;
VerdetData(1,counter)=1/2*atan(2*real(ki)/(1-
abs(ki)^2))*1000;
PhaseData(1,counter)=angle(C3);
EllipData(1,counter)=imag(C4/C3)/(1+abs(ki)^2);
e2AData(counter)=e2A;
e2BData(counter)=e2B;
counter=counter+1;
Lamda=Lamda+WavelengthStep;

end % end of while loop

%%%%%%%%%%%%%%%%%%%%%%%%%%%%%%%%%%%%%%%%%%%%%%%%%%%%%%%%%%%%%%%%%%%%%%%%

% unwinding the phase
for ii=1:length(LamdaRecord)-1
    if (PhaseData(ii+1)-PhaseData(ii))>3
        for jj=ii+1:length(LamdaRecord)
            PhaseData(jj)=PhaseData(jj)-2*pi;
        end
    end
end
end
% end of unwinding the phase

%%%%%%%%%%%%%%%%%%%%%%%%%%%%%%%%%%%%%%%%%%%%%%%%%%%%%%%%%%%%%%%%%%%%%%%%

DelayData=diff(PhaseData)./diff(LamdaRecord);

DelayData(length(DelayData)+1)=DelayData(length(DelayData));

for kk=1:length(LamdaRecord)

    DelayData(kk)=abs(DelayData(kk))*LamdaRecord(kk)*LamdaRecord(kk)*10^-9/(2*pi);

    RotationByDelay(kk)=RotationData(kk)/DelayData(kk);

end

%%%%%%%%%%%%%%%%%%%%%%%%%%%%%%%%%%%%%%%%%%%%%%%%%%%%%%%%%%%%%%%%%%%%%%%%

```

```

AllData=zeros (length (LamdaRecord) , 5);

for RR=1:length (LamdaRecord)
    AllData (RR, 1)=LamdaRecord (RR);
    AllData (RR, 2)=TransData (RR);
    AllData (RR, 3)=VerdetData (RR);
    AllData (RR, 4)=DelayData (RR);
    AllData (RR, 5)=EllipData (RR);
end

%%%%%%%%%%%%%%%%%%%%%%%%%%%%%%%%%%%%%%%%%%%%%%%%%%%%%%%%%%%%%%%%%%%%%%%%

save ('C:\Users\bshakya\Desktop\filename.txt', 'AllData', '-ASCII');
WaveRes;
length (LamdaRecord);
AvgData=zeros (length (LamdaRecord));
FWHM = 4.5;
Delta = FWHM / 2.3548;
WavelengthStep = 0.1;
nopoints=WaveRes-30;

%%%%%%%%%%%%%%%%%%%%%%%%%%%%%%%%%%%%%%%%%%%%%%%%%%%%%%%%%%%%%%%%%%%%%%%%

figure('Name','AvgVerdet VS. wavelength', 'Numbertitle',
'off');
plot (LamdaRecord(30:nopoints), VerdetData(30:nopoints)),
xlabel('Wavelength (nm)'), ylabel('splayer');
grid on

figure('Name','AvgTrans VS. wavelength', 'Numbertitle',
'off');
plot (LamdaRecord(30:nopoints), TransData(30:nopoints)),
xlabel('Wavelength (nm)'), ylabel('splayer');
grid on

end;
% end of seed for-loop

```

REFERENCES

- [1] A. C. Edrington, A. M. Urbas, P. DeRege, C. X. Chen, T. M. Swager, N. Hadjichristidis, M. Xenidou, L. J. Fetters, J. D. Joannopoulos, Y. Fin, and E. L. Thomas, "Polymer-based photonic crystals," - *Adv. Mater*, 13: 421-425, 2001.
- [2] Palash Gangopadhyay, Ramakrishna Voorakaranam, Alejandra Lopez-Santiago, Stijn Foerier, Jayan Thomas, Robert A. Norwood, Andre Persoons, and Nasser Peyghambarian, "Faraday Rotation Measurements on Thin Films of Regioregular Alkyl-Substituted Polythiophene Derivatives," - *J. Phys. Chem*, 112: 8032–8037, 2008.
- [3] Frank J. Loeffler. "A Faraday rotation experiment for undergraduate physics laboratory," - *Am J. Phys*, 51: 661-662, 1983.
- [4] Frank L. Pedrotti and Peter Bandettini, "Faraday rotation in the undergraduate advanced laboratory," - *Am J. Phys*, 58: 542-545, 1990.
- [5] H. Kato, T. Matsushita, A. Takayama, M. Egawa, K. Nishimura, and M. Inoue, "Theoretical analysis of optical a magneto-optical properties of one-dimensional magnetophotonic crystals," - *J. Appl. Phys*, 93: 3906-3911, 2003.
- [6] M. Inoue, K. Arai, T. Fujii, and M. Abe, "One-dimensional magnetophotonic crystals," - *J. Appl. Phys*, 85: 5768-5770, 1999.
- [7] R. Atkinson, "Limits of enhancement of the Faraday effect in ultra-thin magnetic layers by one-dimensional magnetophotonic crystals," - *J. Phys. D: Appl. Phys*, 39: 999-1005, 2006.
- [8] H. Kato, T. Matsushita, A. Takayama, M. Egawa, K. Nishimura, and M. Inoue, "Properties of one-dimensional magnetophotonic crystals for use in optical isolator devices," - *IEEE Trans. Magn*, 38: 3246-3248, 2002.
- [9] H. Y. Ling, "Theoretical investigation of transmission through a Faraday-active Fabry-Perot etalon," - *J. Opt. Soc. Am. A*, 11: 754-758, 1994.
- [10] H. X. Da, J.C. Wu, and Z.Y. Li, "Polarization-independent directional anisotropic optical effect in magnetophotonic crystal," - *Appl. Phys. Lett*, 91: 172515, 2007.
- [11] M. Inoue, K. Arai, T. Fujii, and M. Abe, "Magneto-optical properties of one-dimensional photonic crystals composed of magnetic and dielectric layers," - *J. Appl. Phys*, 83: 6768-6770, 1998.

- [12] S. Sakaguchi and N. Sugimoto, "Transmission Properties of Multilayer Films Composed of Magneto-Optical and Dielectric Materials," - *J. Lightwave Technol*, 17: 1087-1092, 1999.
- [13] B. Wu, F. Lui, S. Lui, and W. Huang, "Research on transmission spectra of one-dimensional magneto-photonic crystals," - *Optoelectron. Lett*, 5: 268-272, 2009.
- [14] A.G. Zhdanov, A. A. Fedyanin, O.A. Aktsipetrov, D. Kobayashi, H. Uchida, and M. Inoue, "Enhancement of Faraday rotation at photonic-band-gap edge in garnet-based magnetophotonic crystals," - *J. Magnetism & Magnetic Mater*, 300: 253-256, 2005.
- [15] A.B. Khanikaev, A.B. Baryshev, P.B. Lim, H. Uchida, M. Inoue, A. G. Zhdanov, A. A. Fedyanin, A.I. Maydykovskiy, and O.A. Aktsipetrov, "Nonlinear Verdet law in magnetophotonic crystals: Interrelation between Faraday and Borrmann effects," - *Phys. Rev B*, 78: 193102-1-193102-4 , 2008.
- [16] M. J. Steel, M. Levy, and R. M. Osgood, "High transmission enhanced Faraday rotation in one-dimensional photonic crystals with defects," - *IEEE Photonics Technol. Lett*, 12: 1171-1173, 2000.
- [17] V.I. Belotelov and A.K. Zvezdin, "Magneto-optical properties of photonic crystals," - *J. Opt. Soc. Am*, 22: 286-292, 2005.
- [18] S. Kahl and A.M. Grishin, "Enhanced Faraday rotation in all-garnet magneto-optical photonic crystal," - *Appl. Phys. Lett*, 84: 1438-1440, 2004.
- [19] S. I. Khartsev and A. M. Grishin, "[Bi₃Fe₅O₁₂/Gd₃Ga₅O₁₂]m magneto-optical photonic crystals," - *Appl. Phys. Lett*. 87: 122504, 2005.
- [20] Yamagata Y., Oshi T., Katsukawa H., Kato S. and Sakurai Y., "Development of optical current transformers and application to fault location systems for substations," - *IEEE Transactions on Power Delivery*, 8: 866-873, 1993.
- [21] Ding W. X., Brower D. L., Deng B. H., Craig D., Prager S. C. and Svidzinski V., "Laser Faraday rotation measurement of current density fluctuations and electromagnetic torque (invited)," - *Review of Scientific Instruments*, 75: 3387-3392, 2004.
- [22] Gongde Li., Kong M.G., Jones, G.R. and Spencer J.W., "Sensitivity improvement of an optical current sensor with enhanced Faraday rotation," - *Journal of Lightwave Technology*, 15: 2246-2252, 1997.
- [23] R. H. Stolen and E.H. Turner, "Faraday rotation in highly birefringent optical fibers," - *Applied Optics*, 19: 842-845, 1980.

- [24] John D. Joannopoulos, Steven G. Johnson, Joshua N. Winn and Robert D. Meade, "Photonic Crystals-Molding the flow of light," - pg 44-45, Princeton University, Princeton, NJ, 2008.
- [25] Leif A. A. Pettersson, Lucimara S. Roman and Olle Inganas, "Modeling photocurrent action of photovoltaic devices based on organic thin films," – *Journal of Applied Physics*, 86: 487-496, 1999.
- [26] V.K. Valev, J. Wouters, and T. Verbiest, "Differential detection for measurements of Faraday rotation by means of ac magnetic fields," - *Euro. J. Phys*, 29: 1099-1104, 2008.
- [27] M.J. Weber, Ed., "Handbook of Optical Materials," - pg. 248, CRC Press, 2003.
- [28] Eugene Hecht, "Optics," - pg 85, Adelphi University, Addison Wesley, CA, 2002
- [29] H.C.Y. Yu, M.A. Van Eijkelenborg, S.G. Leon-Saval, A. Argyros and G.W. Barton, "Enhanced magneto-optical effect in cobalt nanoparticle-doped optical fiber," - *Appl. Opt*, 47: 6497-6501, 2008.
- [30] Paul R. Camp and Richard C. Raymond, "A Photoelectric Polarimeter for Measurement of Transient Rotations," – *J. of the Optical Society of America* , 42: 237-241, 1952.
- [31] L. A. A. Pettersson, L. S. Roman, and O. Inganas, "Modeling photocurrent action spectra of photovoltaic devices based on organic thin films," - *J. Appl. Phys*, 86: 487-496, 1999.
- [32] S.E Caudill and W.T. Grubbs, "Interferometric Measurements of Refractive Index Dispersion in Polymers over the Visible and Near-Infrared Spectral Range," - *J. Appl. Polymer Science*, 100: 65-72, 2006.
- [33] I.D. Nikolov and C.D Ivanov, "Optical Plastic refractive measurements in the visible and the near-infrared regions," - *Appl. Opt*, 39: 2067-2070, 2000.
- [34] R.M.A. Azzam and N.M. Bashara, "Ellipsometry and polarized light," - North-Holland Pub. Co, 1977.
- [35] H. Kato, T. Matsushita, A. Takayama, M. Egawa, K. Nishimura and M. Inoue, "Theoretical analysis of optical a magneto-optical properties of one-dimensional magnetophotonic crystals," - *J. Appl. Phys*, 93: 3906-3911, 2003.